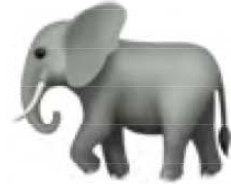


Quantum Error Correction

Fundamental Problem



Quantum States are fragile, especially when entangled

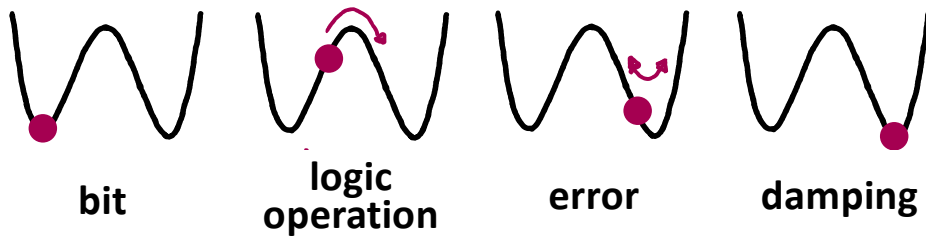
Quantum Computation →

- * Cannot tolerate dissipation
- * Destroys superposition and entanglement

What to do? **Error Correction!**

Classical Computation ?

Dissipation helps



No dissipation →

Errors build up

Classical Error Correction:

Simple example: Redundancy protects against bit flips

Encode:
 $0 \rightarrow (000)$
 $1 \rightarrow (111)$

Errors:
 $(000) \rightarrow (100)$
 $(111) \rightarrow (011)$ correct by majority vote

Quantum Computation

- * Cannot tolerate dissipation
- * Destroys superposition and entanglement

What to do? **Error Correction!**

Classical Error Correction:

Simple example: Redundancy protects against bit flips



Encode: $0 \rightarrow (000)$
 $1 \rightarrow (111)$

Errors: $(000) \rightarrow (100)$
 $(111) \rightarrow (011)$ correct by majority vote

Von Neumann:

- * A classical computer w/faulty components can work, given enough redundancy
- * Classical error correction is well developed and highly sophisticated...

* Quantum Errors

- 1) Bit Flip $|0\rangle \rightarrow |1\rangle$, phase flip $|0\rangle \rightarrow |0\rangle$
 $|1\rangle \rightarrow |0\rangle$, $|1\rangle \rightarrow -|1\rangle$
- 2) Small errors $a|0\rangle + b|1\rangle$ a, b can change by ϵ
errors accumulate
- 3) Measurement disturbs  collapse of quantum states
- 4) No cloning  Cannot protect by making copies

Von Neumann:

- * A classical computer w/faulty components can work, given enough redundancy
- * Classical error correction is well developed and highly sophisticated...

* Quantum Errors

- 1) Bit Flip $|0\rangle \rightarrow |1\rangle$, phase flip $|0\rangle \rightarrow |0\rangle$
 $|1\rangle \rightarrow |0\rangle$, $|1\rangle \rightarrow -|1\rangle$
- 2) Small errors $a|0\rangle + b|1\rangle$ a, b can change by ϵ
 errors accumulate
- 3) Measurement disturbs \Rightarrow collapse of quantum states
- 4) No cloning \Rightarrow Cannot protect by making copies

Example: Peter Shor's code for bit flip error when $P(\text{error}) \ll 1$

Encode: $|0\rangle \rightarrow |0\rangle \equiv |000\rangle$ (3 bit code)
 $|1\rangle \rightarrow |1\rangle \equiv |111\rangle$

$$a|0\rangle + b|1\rangle \rightarrow a|000\rangle + b|111\rangle$$

Single-qubit measurement \Rightarrow

collapse of state, destroys info, no majority voting!

Collective 2-qubit measurement:

- for $|x, y, z\rangle$ measure $y \oplus z$ (never measure individual bits)
 $x \oplus z$
- if $|000\rangle, |111\rangle$ these observables = 0
- if one bit-flip, at least one observable = 1
- easy to check that $(y \oplus z, x \oplus z) =$ binary address of qubit flip

$$|000\rangle \rightarrow |010\rangle \quad (1, 0) = \text{2nd bit}$$

Introduction and Overview (Preskills Notes)

9-03-2024

Example: Peter Shor's code for bit flip error when $P(\text{error}) \ll 1$

Encode: $|0\rangle \rightarrow |\bar{0}\rangle \equiv |000\rangle$ (3 bit code)
 $|1\rangle \rightarrow |\bar{1}\rangle \equiv |111\rangle$



$$a|0\rangle + b|1\rangle \rightarrow a|000\rangle + b|111\rangle$$

Single-qubit measurement



collapse of state, destroys info, no majority voting!

Collective 2-qubit measurement:

- for $|x, y, z\rangle$ measure $y \oplus z$ (never measure individual bits)
 $x \oplus z$

- if $|000\rangle, |111\rangle$ these observables = 0

- if one bit-flip, at least one observable = 1

- easy to check that $(y \oplus z, x \oplus z) =$ binary address of qubit flip

$$|000\rangle \rightarrow |010\rangle \quad (1, 0) = \text{2nd bit}$$

Small errors: $|000\rangle \rightarrow |000\rangle + \epsilon|100\rangle$
 $|111\rangle \rightarrow |111\rangle + \epsilon|110\rangle$

Quantum mechanics to the rescue !

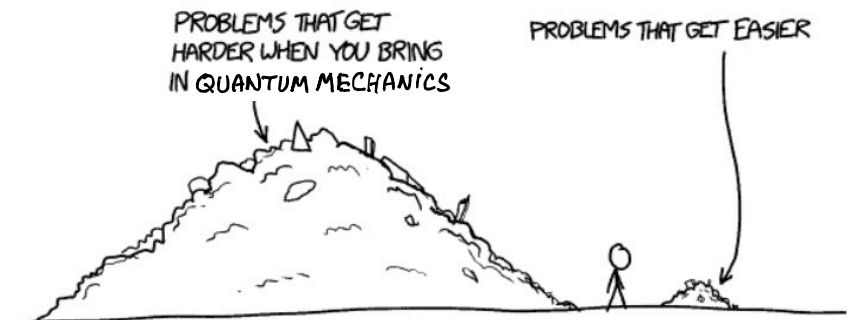
- mostly no error detected

➡ collapse into $|000\rangle$ resp. $|111\rangle$

- sometime error detected

➡ collapse into $|001\rangle$ resp. $|110\rangle$

➡ full bit flip, correct as such



Source: xkcd.com

Example: Peter Shor's code for bit flip error when $P(\text{error}) \ll 1$

Encode: $|0\rangle \rightarrow |\bar{0}\rangle \equiv |000\rangle$ (3 bit code)
 $|1\rangle \rightarrow |\bar{1}\rangle \equiv |111\rangle$



$$a|0\rangle + b|1\rangle \rightarrow a|000\rangle + b|111\rangle$$

Single-qubit measurement



collapse of state, destroys info, no majority voting!

Collective 2-qubit measurement:

- for $|x, y, z\rangle$ measure $y \oplus z$ (never measure individual bits)
 $x \oplus z$

- if $|000\rangle, |111\rangle$ these observables = 0

- if one bit-flip, at least one observable = 1

- easy to check that $(y \oplus z, x \oplus z) =$ binary address of qubit flip

$$|000\rangle \rightarrow |010\rangle \quad (1, 0) = \text{2nd bit}$$

Small errors: $|000\rangle \rightarrow |000\rangle + \epsilon|100\rangle$
 $|111\rangle \rightarrow |111\rangle + \epsilon|110\rangle$

Quantum mechanics to the rescue !

- mostly no error detected

➡ collapse into $|000\rangle$ resp. $|111\rangle$

- sometime error detected

➡ collapse into $|001\rangle$ resp. $|110\rangle$

➡ full bit flip, correct as such

How to implement ?

Quantum circuit + single qubit measurement

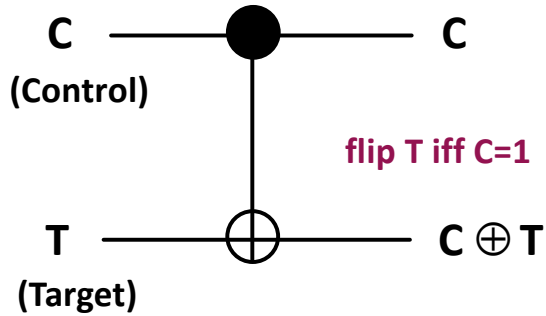
Quantum Gates – work on superpositions, and entangled states

Introduction and Overview (Preskills Notes)

9-05-2024

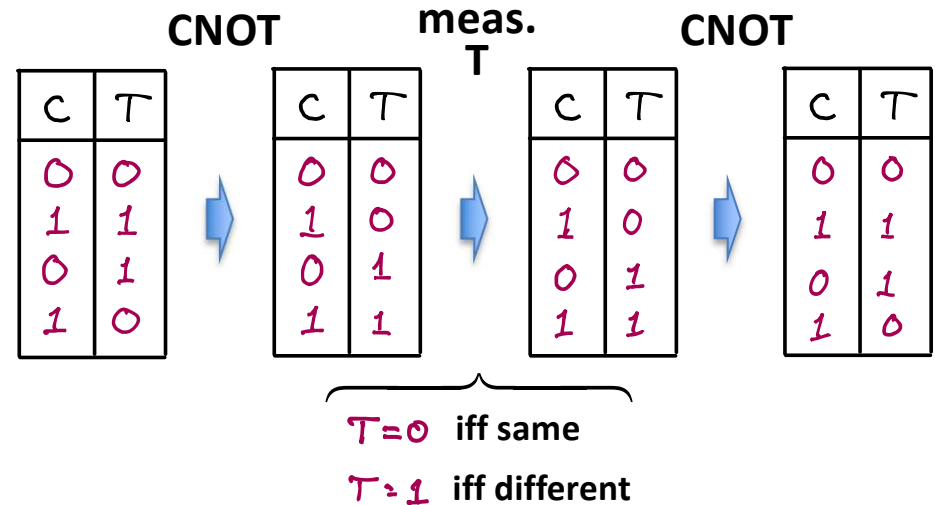
Controlled-NOT (CNOT)

Truth Table

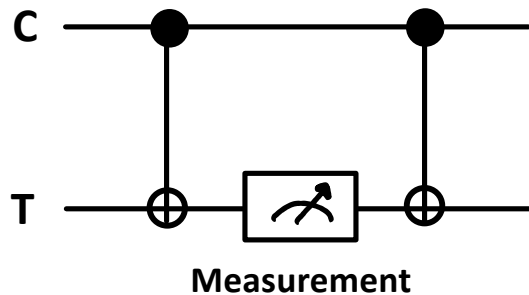


C	T	$C \oplus T$
0	0	0
0	1	1
1	0	1
1	1	0

Circuit maps logical basis states as

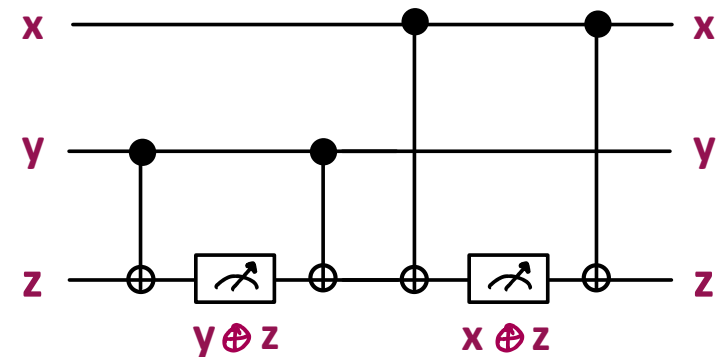


Quantum Circuit for joint measurement



Measurement in $\{|0\rangle, |1\rangle\}$ basis yields $C \oplus T$

Full circuit to obtain Error Syndrome

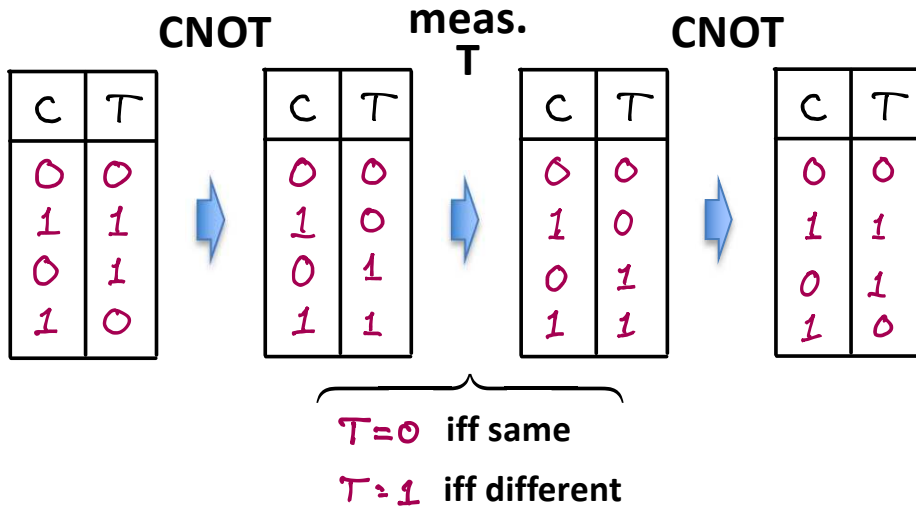


* iff qubit flip, binary address = $(y \oplus z, x \oplus z)$

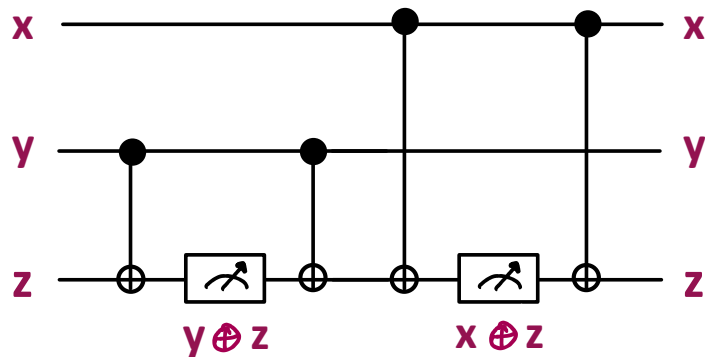
Introduction and Overview (Preskills Notes)

9-05-2024

Circuit maps logical basis states as



Full circuit to obtain Error Syndrome



* iif qubit flip, binary address = $(y \oplus z, x \oplus z)$

Quantum Phase Error

$$|0\rangle \rightarrow |0\rangle$$

$$|1\rangle \rightarrow -|1\rangle$$

Encoding

$$|0\rangle \rightarrow |\bar{0}\rangle = \frac{1}{2^{3/2}} (|0\rangle + |1\rangle)^{x'} (|0\rangle + |1\rangle)^{y'} (|0\rangle + |1\rangle)^{z'}$$

$$|1\rangle \rightarrow |\bar{1}\rangle = \frac{1}{2^{3/2}} (|0\rangle - |1\rangle)^{x'} (|0\rangle - |1\rangle)^{y'} (|0\rangle - |1\rangle)^{z'}$$

Relabel

$$\frac{1}{\sqrt{2}} (|0\rangle + |1\rangle) = |0'\rangle$$

$$\frac{1}{\sqrt{2}} (|0\rangle - |1\rangle) = |1'\rangle$$

Measure in basis

$$\{|0'\rangle, |1'\rangle\} \rightarrow y' \oplus z', x' \oplus z'$$

Error Syndrome

* Iff phase error, binary address = $(y' \oplus z', x' \oplus z')$

* Analogous to bit-flip code, just in different basis

Quantum Phase Error $|0\rangle \rightarrow |0\rangle$
 $|1\rangle \rightarrow -|1\rangle$

Encoding

$$|0\rangle \rightarrow |\bar{0}\rangle = \frac{1}{2^{3/2}} (|0\rangle + |1\rangle) (|0\rangle + |1\rangle) (|0\rangle + |1\rangle)$$

$$|1\rangle \rightarrow |\bar{1}\rangle = \frac{1}{2^{3/2}} (|0\rangle - |1\rangle) (|0\rangle - |1\rangle) (|0\rangle - |1\rangle)$$

Relabel $\frac{1}{\sqrt{2}} (|0\rangle + |1\rangle) = |0'\rangle$
 $\frac{1}{\sqrt{2}} (|0\rangle - |1\rangle) = |1'\rangle$

Measure in basis $\{|0'\rangle, |1'\rangle\} \rightarrow y' \oplus z', x' \oplus z'$

Error Syndrome

- * Iff phase error, binary address = $(y' \oplus z', x' \oplus z')$
- * Analogous to bit-flip code, just in different basis

Shor's 9-bit code

- * Combines flip/phase error correction
- * Corrects one flip or phase error

General principle of error correction

- * Encode p logical qubits in n physical qubits.
- * Valid Logical States form 2^p -dimensional subspace \mathcal{E}_p (code space) in n -qubit (2^n -dimensional) Hilbert space \mathcal{E}_n
- * Errors displace system into orthogonal (distinguishable) subspaces.

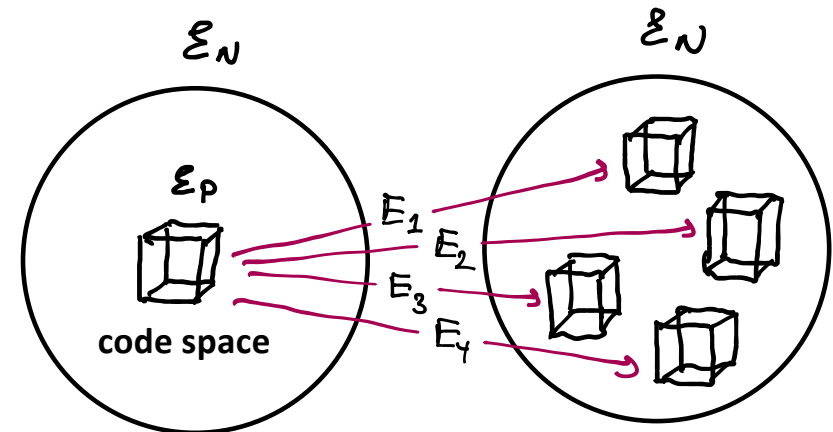
Shor's 9-bit code

- * Combines flip/phase error correction
- * Corrects one flip or phase error

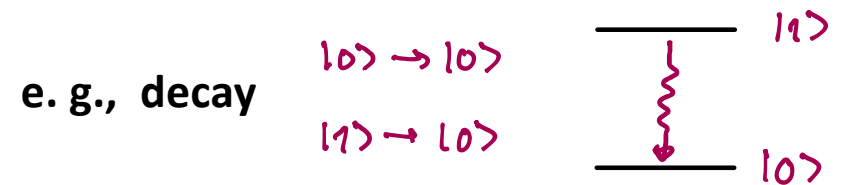
General principle of error correction

- * Encode p logical qubits in n physical qubits.
- * Valid Logical States form 2^p -dimensional subspace \mathcal{E}_p (code space) in n -qubit (2^n -dimensional) Hilbert space \mathcal{E}_n
- * Errors displace system into orthogonal (distinguishable) subspaces.

Geometric illustration



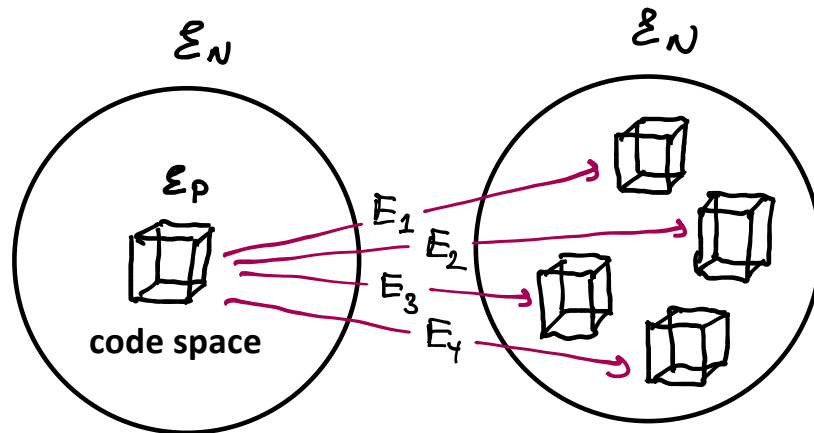
What about non-Unitary errors?



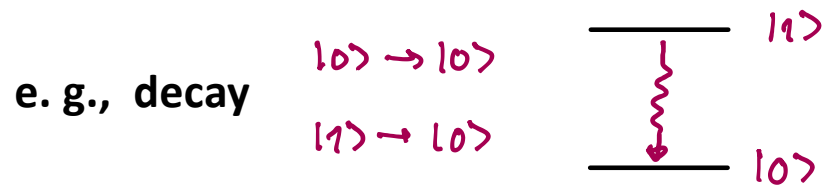
- Problem: Errors not displaced into orthogonal subspaces
- Solution: "Quantum jump codes", monitors the environment

Other kinds of errors?

Geometric illustration



What about non-Unitary errors?



Problem: Errors not displaced into orthogonal subspaces

Solution: "Quantum jump codes", monitors the environment

Other kinds of errors?

Introduction and Overview (Preskills Notes)

9-05-2024

Catnip for Theoretical Physicists & Computer Scientists

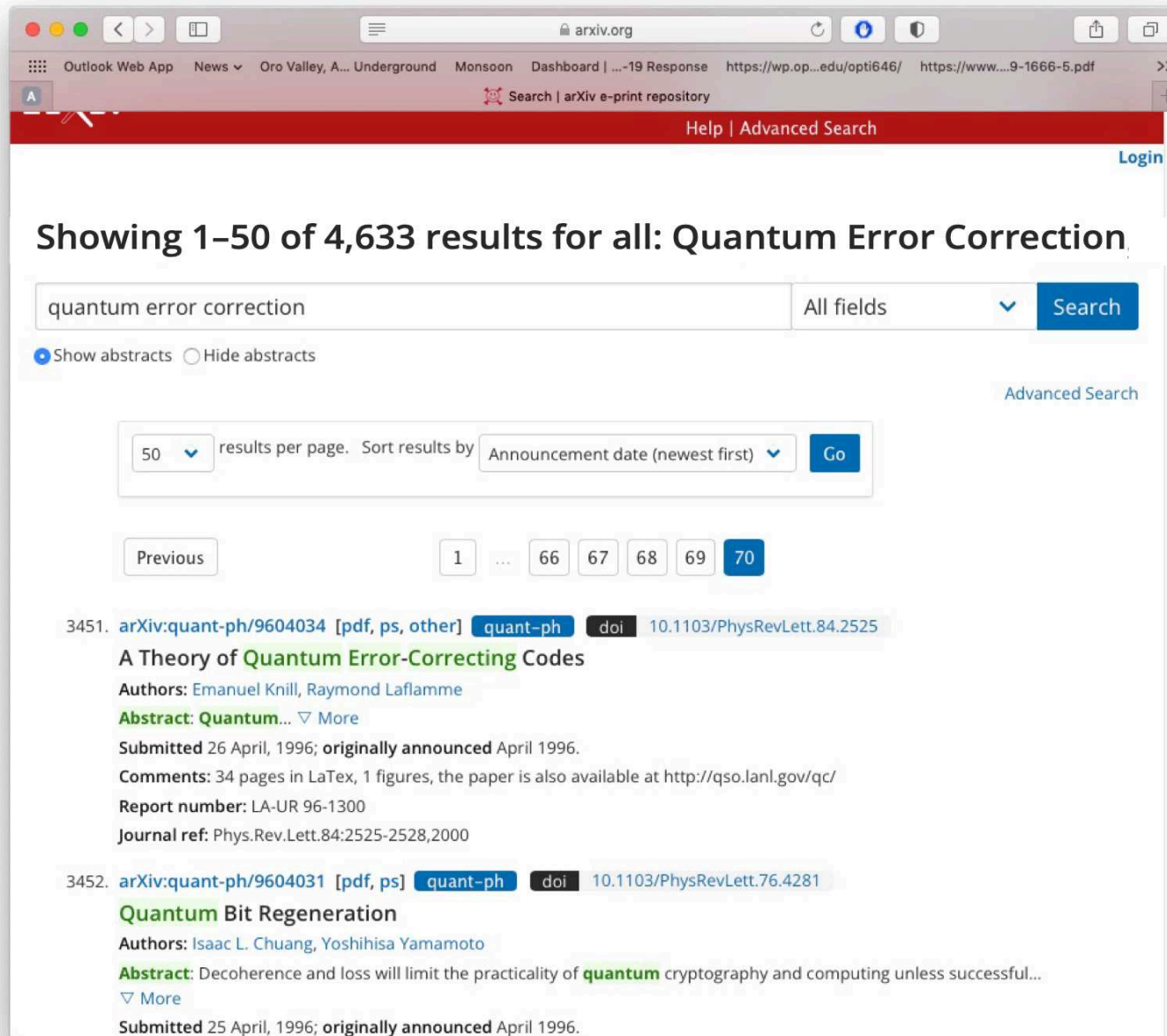
The screenshot shows the arXiv search results page for the query "quantum error correction". The page displays 3,479 results, with the current view showing results 3451 to 3479. The search results are sorted by "Announcement date (newest first)" and are displayed in a list format. The first two results are highlighted:

- 3451. [arXiv:quant-ph/9604034](https://arxiv.org/abs/quant-ph/9604034) [pdf, ps, other] [quant-ph](#) [doi](#) 10.1103/PhysRevLett.84.2525
A Theory of Quantum Error-Correcting Codes
Authors: Emanuel Knill, Raymond Laflamme
Abstract: Quantum... [More](#)
Submitted 26 April, 1996; originally announced April 1996.
Comments: 34 pages in LaTeX, 1 figures, the paper is also available at <http://qso.lanl.gov/qc/>
Report number: LA-UR 96-1300
Journal ref: Phys.Rev.Lett.84:2525-2528,2000
- 3452. [arXiv:quant-ph/9604031](https://arxiv.org/abs/quant-ph/9604031) [pdf, ps] [quant-ph](#) [doi](#) 10.1103/PhysRevLett.76.4281
Quantum Bit Regeneration
Authors: Isaac L. Chuang, Yoshihisa Yamamoto
Abstract: Decoherence and loss will limit the practicality of quantum cryptography and computing unless successful...
[More](#)
Submitted 25 April, 1996; originally announced April 1996.

Introduction and Overview (Preskills Notes)

9-05-2024

Catnip for Theoretical Physicists & Computer Scientists



The screenshot shows the arXiv search results page for the query "quantum error correction". The page displays 4,633 results, with the first two results visible. The search interface includes a search bar, a "Search" button, and options to show or hide abstracts. The results are sorted by "Announcement date (newest first)" and are displayed in a list format. The first result is "A Theory of Quantum Error-Correcting Codes" by Emanuel Knill and Raymond Laflamme, submitted on 26 April 1996. The second result is "Quantum Bit Regeneration" by Isaac L. Chuang and Yoshihisa Yamamoto, submitted on 25 April 1996.

Showing 1–50 of 4,633 results for all: Quantum Error Correction

quantum error correction All fields Search

Show abstracts Hide abstracts

Advanced Search

50 results per page. Sort results by Announcement date (newest first) Go

Previous 1 ... 66 67 68 69 70

3451. [arXiv:quant-ph/9604034](https://arxiv.org/abs/quant-ph/9604034) [pdf, ps, other] [quant-ph](#) [doi](#) 10.1103/PhysRevLett.84.2525

A Theory of Quantum Error-Correcting Codes

Authors: Emanuel Knill, Raymond Laflamme

Abstract: Quantum... [More](#)

Submitted 26 April, 1996; originally announced April 1996.

Comments: 34 pages in LaTeX, 1 figures, the paper is also available at <http://qso.lanl.gov/qc/>

Report number: LA-UR 96-1300

Journal ref: Phys.Rev.Lett.84:2525-2528,2000

3452. [arXiv:quant-ph/9604031](https://arxiv.org/abs/quant-ph/9604031) [pdf, ps] [quant-ph](#) [doi](#) 10.1103/PhysRevLett.76.4281

Quantum Bit Regeneration

Authors: Isaac L. Chuang, Yoshihisa Yamamoto

Abstract: Decoherence and loss will limit the practicality of quantum cryptography and computing unless successful... [More](#)

Submitted 25 April, 1996; originally announced April 1996.

Quantum Hardware

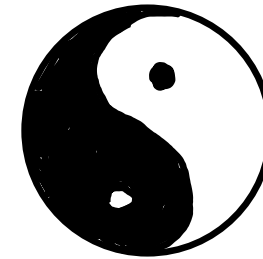
Physical Implementation is
Extremely demanding !

Requirements

1. Storage: Quantum memory.
2. Gates: We put computation U_f together from 1 and 2-qubit operations.
3. Readout: Method to measure qubits.
4. Isolation: No coupling to environment to avoid decoherence & errors
5. Precision: Gates, readouts must be highly accurate

Inherent Contradictions

2. Gates **vs** 4. Isolation
- ↑ ↑
- coupling between qubits no coupling to environment



To build a Quantum Computer:

Choose, find or invent a system with acceptable tradeoffs.

6. Error Correction must not create more errors than it corrects.



7. Thresholds for Error Correction and Fault Tolerance

Quantum Computing in the NISQ era and beyond

John Preskill

Institute for Quantum Information and Matter and Walter Burke Institute for Theoretical Physics,
California Institute of Technology, Pasadena CA 91125, USA

30 July 2018

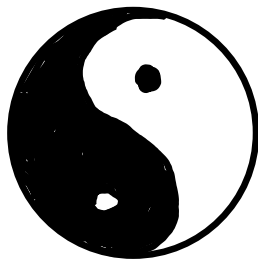
Noisy Intermediate-Scale Quantum (NISQ) technology will be available in the near future. Quantum computers with 50-100 qubits may be able to perform tasks which surpass the capabilities of today's classical digital computers, but noise in quantum gates will limit the size of quantum circuits that can be executed reliably. NISQ devices will be useful tools for exploring many-body quantum physics, and may have other useful applications, but the 100-qubit quantum computer will not change the world right away — we should regard it as a significant step toward the more powerful quantum technologies of the future. Quantum technologists should continue to strive for more accurate quantum gates and, eventually, fully fault-tolerant quantum computing.

Inherent Contradictions

2. Gates **vs** 4. Isolation

↑ ↑

coupling between qubits no coupling to environment



To build a Quantum Computer:

Choose, find or invent a system with acceptable tradeoffs.

6. Error Correction must not create more errors than it corrects.

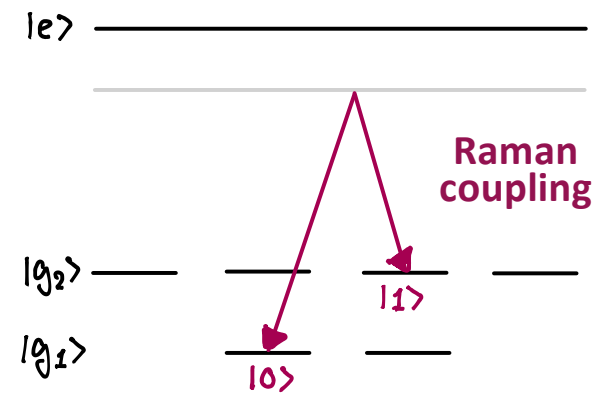


7. Thresholds for Error Correction and Fault Tolerance

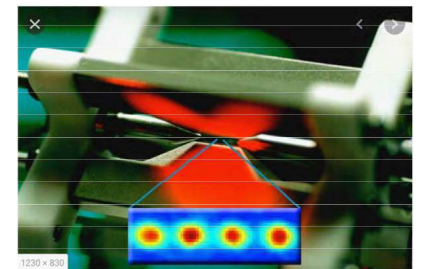
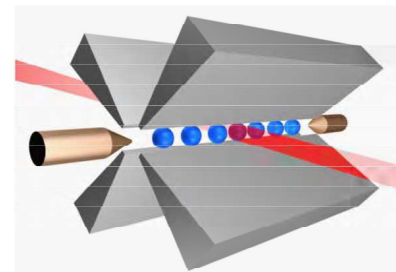
Ion Trap Quantum Computing

First to demonstrate a Quantum Gate

* Qubit is encoded in the electronic ground state of an atomic ion



* Early design with a few ions in large trap

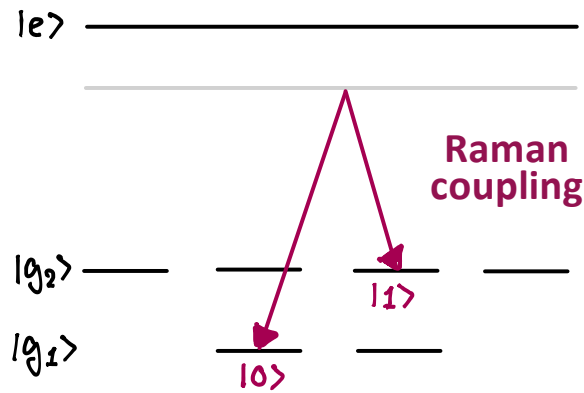


Introduction and Overview (Preskills Notes)

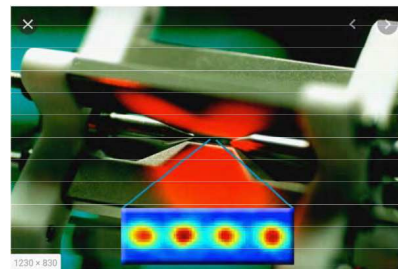
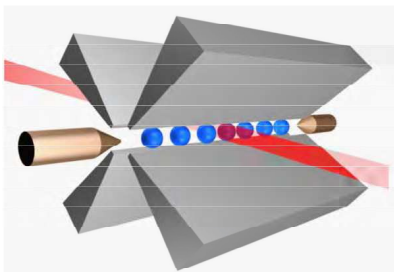
Ion Trap Quantum Computing

First to demonstrate a Quantum Gate

- * Qubit is encoded in the electronic ground state of an atomic ion



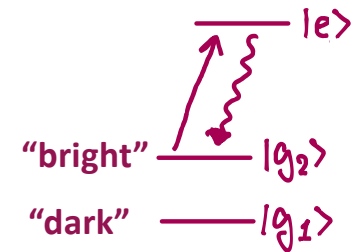
- * Early design with a few ions in large trap



Requirements

1. Storage: 10s-100s coherence time
2. Gates: Use collective vibrations as "quantum bus"

3. Readout: Fluorescence



Cirac & Zoller: 5 laser pulses

CNOT gate between any 2 ions in linear array

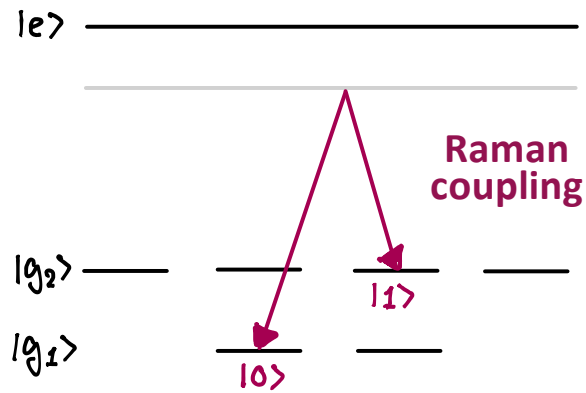
Wineland: 3 laser pulses enough for CNOT

Use this example serves as conceptual template

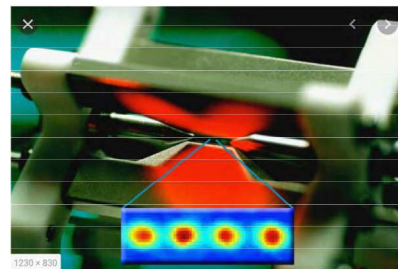
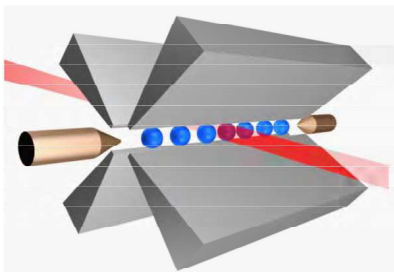
Ion Trap Quantum Computing

First to demonstrate a Quantum Gate

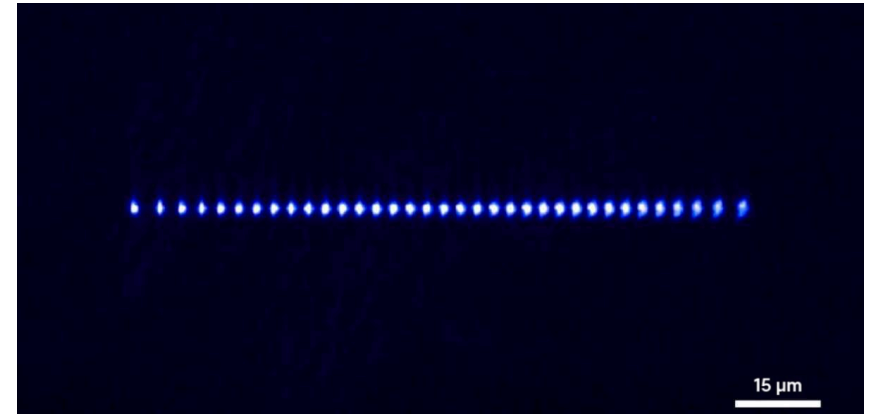
- * Qubit is encoded in the electronic ground state of an atomic ion



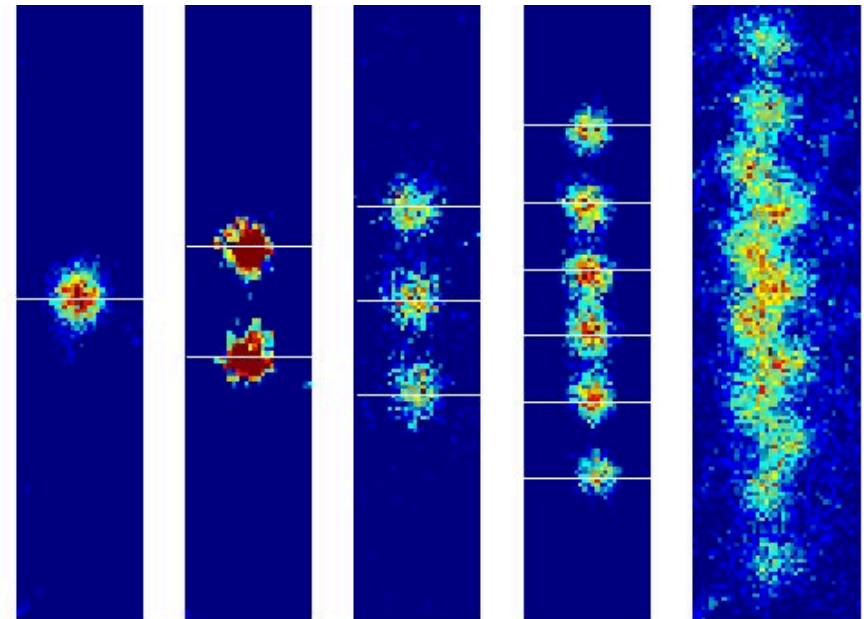
- * Early design with a few ions in large trap



- * Scaling up in Linear Ion Traps



- * Limitations



Status: Many important milestones achieved

- * Entanglement of ≥ 20 ions (2018)
- * Highest gate & readout fidelities, longest coherence times
- * Error Correction, Fault Tolerance proof of principle demonstrations
- * Complex algorithms on few ions, quantum simulations with ≥ 50
- * Research groups in academia, National Labs, Industry

Some early leaders

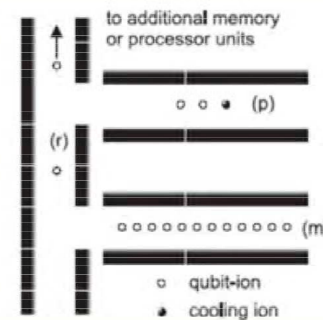
NIST Innsbruck Quantinuum

Sandia NL Duke U IonQ

Many others these days

- * Major challenges – same as late 2000’s!
- * “Clock speed” set by vibrational freqs microfabricated traps do better
- * More ions -> harder to cool motion, harder to individually address ions in linear trap.
- * Scaling up to 1000’s of ions is an enormous challenge

Scalable Ion Trap Quantum Processor – one vision



D. Kielpinski, C. Monroe, and D. J. Wineland, Nature 417, 709 (2002).

To appear in the 2007 International Symposium on Microarchitecture (MICRO-31)
A Quantum Logic Array Microarchitecture: Scalable Quantum Data Movement and Computation

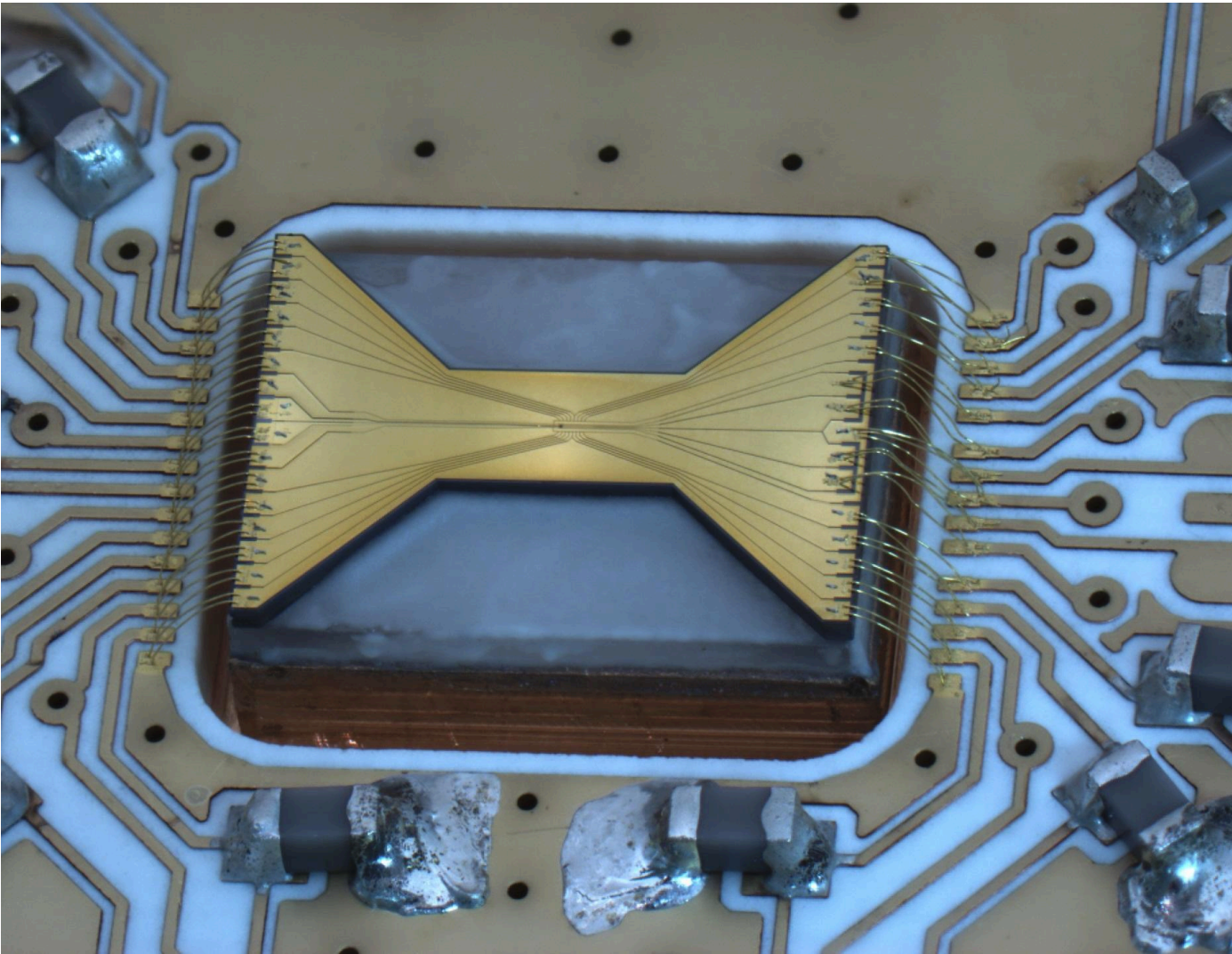
Tzvetan S. Metodi¹, Darshan D. Thaker¹, Andrew W. Cross²
Frederic T. Chong¹ and Isaac L. Chuang²

Operation	Time	$P_{current}$	$P_{expected}$
Single Gate	1 μ s	0.0001	10 ⁻⁸
Double Gate	10 μ s	0.03	10 ⁻⁷
Measure	100 μ s	0.01	10 ⁻⁸
Movement	10ns/ μ m	0.005/ μ m	10 ⁻⁶ /cell
Split	10 μ s		
Cooling	1 μ s		
Memory time	10 – 100 sec		

Introduction and Overview (Preskills Notes)

9-10-2024

NIST Group, Current as of 2023



Demonstration of a Fundamental Quantum Logic Gate

C. Monroe, D. M. Meekhof, B. E. King, W. M. Itano, and D. J. Wineland

National Institute of Standards and Technology, Boulder, Colorado 80303

(Received 14 July 1995)

We demonstrate the operation of a two-bit “controlled-NOT” quantum logic gate, which, in conjunction with simple single-bit operations, forms a universal quantum logic gate for quantum computation. The two quantum bits are stored in the internal and external degrees of freedom of a single trapped atom, which is first laser cooled to the zero-point energy. Decoherence effects are identified for the operation, and the possibility of extending the system to more qubits appears promising.

Introduction and Overview (Preskills Notes)

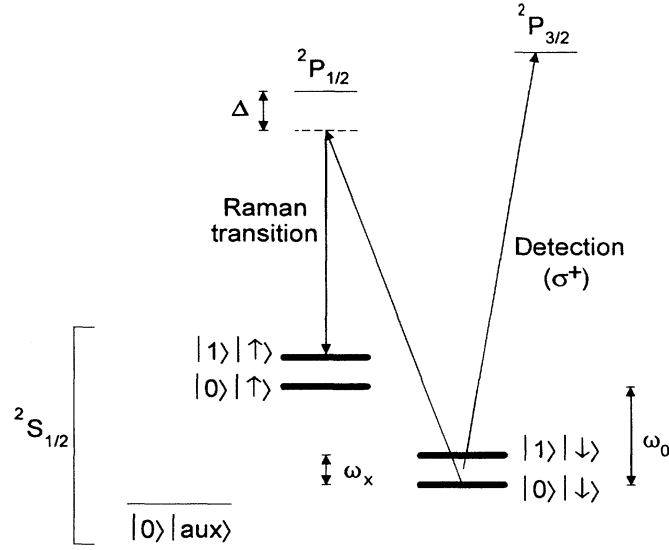


FIG. 1. ${}^9\text{Be}^+$ energy levels. The levels indicated with thick lines form the basis of the quantum register: internal levels are $|S\rangle = |\downarrow\rangle$ and $|\uparrow\rangle$ (${}^2S_{1/2}|F=2, m_F=2\rangle$ and ${}^2S_{1/2}|F=1, m_F=1\rangle$ levels, respectively, separated by $\omega_0/2\pi \approx 1.250$ GHz), and $|\text{aux}\rangle = {}^2S_{1/2}|F=2, m_F=0\rangle$ (separated from $|\downarrow\rangle$ by ≈ 2.5 MHz); external vibrational levels are $|n\rangle = |0\rangle$ and $|1\rangle$ (separated by $\omega_x/2\pi \approx 11.2$ MHz). Stimulated Raman transitions between ${}^2S_{1/2}$ hyperfine states are driven through the virtual ${}^2P_{1/2}$ level ($\Delta \approx 50$ GHz) with a pair of ≈ 313 nm laser beams. Measurement of S is accomplished by driving the cycling $|\downarrow\rangle \rightarrow {}^2P_{3/2}|F=3, m_F=3\rangle$ transition with σ^+ -polarized light and detecting the resulting ion fluorescence.

according to the following format:

- A $\pi/2$ pulse is applied on the carrier transition. The effect is described by the operator $V^{1/2}(\pi/2)$ in the notation of Ref. [1].
- A 2π pulse is applied on the blue sideband transition between $|\uparrow\rangle$ and an auxiliary atomic level $|\text{aux}\rangle$ (see Fig. 1).
- A $\pi/2$ pulse is applied on the carrier transition, with a π phase shift relative to (a), leading to the operator $V^{1/2}(-\pi/2)$ of Ref. [1].

is as follows:

Input state	Output state	
$ 0\rangle \downarrow\rangle$	$\rightarrow 0\rangle \downarrow\rangle$	
$ 0\rangle \uparrow\rangle$	$\rightarrow 0\rangle \uparrow\rangle$	(2)
$ 1\rangle \downarrow\rangle$	$\rightarrow 1\rangle \uparrow\rangle$	
$ 1\rangle \uparrow\rangle$	$\rightarrow 1\rangle \downarrow\rangle$	

The experiment apparatus is described elsewhere [16,17]. A single ${}^9\text{Be}^+$ ion is stored in a coaxial-resonator rf-ion trap [17], which provides pseudopotential oscillation frequencies of $(\omega_x, \omega_y, \omega_z)/2\pi \approx (11.2, 18.2, 29.8)$ MHz along the principal axes of the trap. We cool the ion so that the $n_x = 0$ vibrational ground state is occupied $\approx 95\%$ of the time by employing resolved-sideband stimulated Raman cooling in the x dimension, exactly as in Ref. [16]. The two Raman beams each contain ≈ 1 mW of power at ≈ 313 nm and are detuned ≈ 50 GHz red of the ${}^2P_{1/2}$ excited state. The Raman beams are applied to the ion in directions such that their wave-vector difference $\delta\mathbf{k}$ points nearly along the x axis of the trap; thus the Raman transitions are highly insensitive to motion in the other two dimensions. The Lamb-Dicke parameter is $\eta_x = \delta k x_0 \approx 0.2$, where $x_0 \approx 7$ nm is the spread of the $n_x = 0$ wave function. The carrier ($|n\rangle|\downarrow\rangle \rightarrow |n\rangle|\uparrow\rangle$) Rabi frequency is $\Omega_0 2\pi \approx 140$ kHz, the red ($|1\rangle|\downarrow\rangle \rightarrow |0\rangle|\uparrow\rangle$) and blue ($|0\rangle|\downarrow\rangle \rightarrow |1\rangle|\uparrow\rangle$) sideband Rabi frequencies are $\eta_x \Omega_0 / 2\pi \approx 30$ kHz, and the auxiliary transition ($|1\rangle|\uparrow\rangle \rightarrow |0\rangle|\downarrow\rangle$) Rabi frequency is $\eta_x \Omega_{\text{aux}} / 2\pi \approx 12$ kHz. The difference frequency of the Raman beams is tunable from 1200 to 1300 MHz with the use of a double pass acousto-optic modulator (AOM), and the Raman pulse durations are controlled with additional switching AOMs. Since the Raman beams are generated from a single laser and an AOM, broadening of the Raman transitions due to a finite laser linewidth is negligible [18].

Following Raman cooling to the $|0\rangle|\downarrow\rangle$ state, but before application of the CN operation, we apply appropriately

Introduction and Overview (Preskills Notes)

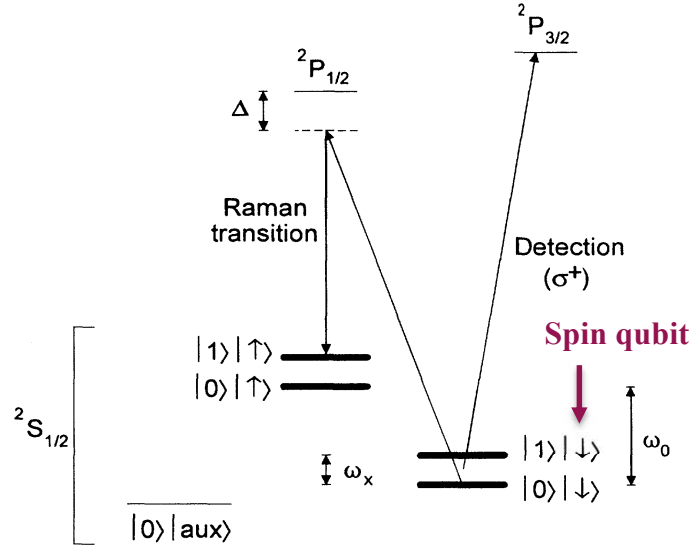


FIG. 1. ${}^9\text{Be}^+$ energy levels. The levels indicated with thick lines form the basis of the quantum register: internal levels are $|S\rangle = |\downarrow\rangle$ and $|\uparrow\rangle$ (${}^2S_{1/2}|F=2, m_F=2\rangle$ and ${}^2S_{1/2}|F=1, m_F=1\rangle$ levels, respectively, separated by $\omega_0/2\pi \approx 1.250$ GHz), and $|\text{aux}\rangle = {}^2S_{1/2}|F=2, m_F=0\rangle$ (separated from $|\downarrow\rangle$ by ≈ 2.5 MHz); external vibrational levels are $|n\rangle = |0\rangle$ and $|1\rangle$ (separated by $\omega_x/2\pi \approx 11.2$ MHz). Stimulated Raman transitions between ${}^2S_{1/2}$ hyperfine states are driven through the virtual ${}^2P_{1/2}$ level ($\Delta \approx 50$ GHz) with a pair of ≈ 313 nm laser beams. Measurement of S is accomplished by driving the cycling $|\downarrow\rangle \rightarrow {}^2P_{3/2}|F=3, m_F=3\rangle$ transition with σ^+ -polarized light and detecting the resulting ion fluorescence.

according to the following format:

- A $\pi/2$ pulse is applied on the carrier transition. The effect is described by the operator $V^{1/2}(\pi/2)$ in the notation of Ref. [1].
- A 2π pulse is applied on the blue sideband transition between $|\uparrow\rangle$ and an auxiliary atomic level $|\text{aux}\rangle$ (see Fig. 1).
- A $\pi/2$ pulse is applied on the carrier transition, with a π phase shift relative to (a), leading to the operator $V^{1/2}(-\pi/2)$ of Ref. [1].

is as follows:

Input state	Output state	
$ 0\rangle \downarrow\rangle$	$\rightarrow 0\rangle \downarrow\rangle$	
$ 0\rangle \uparrow\rangle$	$\rightarrow 0\rangle \uparrow\rangle$	(2)
$ 1\rangle \downarrow\rangle$	$\rightarrow 1\rangle \uparrow\rangle$	
$ 1\rangle \uparrow\rangle$	$\rightarrow 1\rangle \downarrow\rangle$	

The experiment apparatus is described elsewhere [16,17]. A single ${}^9\text{Be}^+$ ion is stored in a coaxial-resonator rf-ion trap [17], which provides pseudopotential oscillation frequencies of $(\omega_x, \omega_y, \omega_z)/2\pi \approx (11.2, 18.2, 29.8)$ MHz along the principal axes of the trap. We cool the ion so that the $n_x = 0$ vibrational ground state is occupied $\approx 95\%$ of the time by employing resolved-sideband stimulated Raman cooling in the x dimension, exactly as in Ref. [16]. The two Raman beams each contain ≈ 1 mW of power at ≈ 313 nm and are detuned ≈ 50 GHz red of the ${}^2P_{1/2}$ excited state. The Raman beams are applied to the ion in directions such that their wave-vector difference $\delta\mathbf{k}$ points nearly along the x axis of the trap; thus the Raman transitions are highly insensitive to motion in the other two dimensions. The Lamb-Dicke parameter is $\eta_x = \delta k x_0 \approx 0.2$, where $x_0 \approx 7$ nm is the spread of the $n_x = 0$ wave function. The carrier ($|n\rangle|\downarrow\rangle \rightarrow |n\rangle|\uparrow\rangle$) Rabi frequency is $\Omega_0 2\pi \approx 140$ kHz, the red ($|1\rangle|\downarrow\rangle \rightarrow |0\rangle|\uparrow\rangle$) and blue ($|0\rangle|\downarrow\rangle \rightarrow |1\rangle|\uparrow\rangle$) sideband Rabi frequencies are $\eta_x \Omega_0 / 2\pi \approx 30$ kHz, and the auxiliary transition ($|1\rangle|\uparrow\rangle \rightarrow |0\rangle|\downarrow\rangle$) Rabi frequency is $\eta_x \Omega_{\text{aux}} / 2\pi \approx 12$ kHz. The difference frequency of the Raman beams is tunable from 1200 to 1300 MHz with the use of a double pass acousto-optic modulator (AOM), and the Raman pulse durations are controlled with additional switching AOMs. Since the Raman beams are generated from a single laser and an AOM, broadening of the Raman transitions due to a finite laser linewidth is negligible [18].

Following Raman cooling to the $|0\rangle|\downarrow\rangle$ state, but before application of the CN operation, we apply appropriately

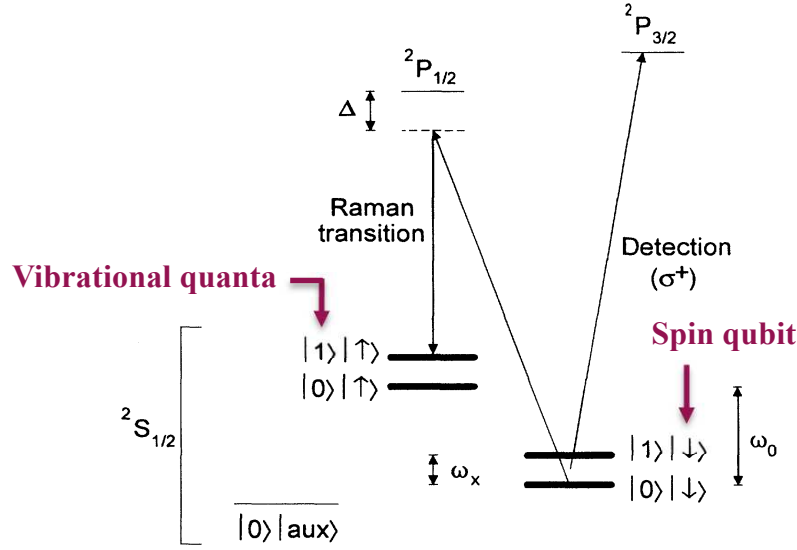


FIG. 1. ${}^9\text{Be}^+$ energy levels. The levels indicated with thick lines form the basis of the quantum register: internal levels are $|S\rangle = |\downarrow\rangle$ and $|\uparrow\rangle$ (${}^2S_{1/2}|F=2, m_F=2\rangle$ and ${}^2S_{1/2}|F=1, m_F=1\rangle$ levels, respectively, separated by $\omega_0/2\pi \approx 1.250$ GHz), and $|\text{aux}\rangle = {}^2S_{1/2}|F=2, m_F=0\rangle$ (separated from $|\downarrow\rangle$ by ≈ 2.5 MHz); external vibrational levels are $|n\rangle = |0\rangle$ and $|1\rangle$ (separated by $\omega_x/2\pi \approx 11.2$ MHz). Stimulated Raman transitions between ${}^2S_{1/2}$ hyperfine states are driven through the virtual ${}^2P_{1/2}$ level ($\Delta \approx 50$ GHz) with a pair of ≈ 313 nm laser beams. Measurement of S is accomplished by driving the cycling $|\downarrow\rangle \rightarrow {}^2P_{3/2}|F=3, m_F=3\rangle$ transition with σ^+ -polarized light and detecting the resulting ion fluorescence.

according to the following format:

- A $\pi/2$ pulse is applied on the carrier transition. The effect is described by the operator $V^{1/2}(\pi/2)$ in the notation of Ref. [1].
- A 2π pulse is applied on the blue sideband transition between $|\uparrow\rangle$ and an auxiliary atomic level $|\text{aux}\rangle$ (see Fig. 1).
- A $\pi/2$ pulse is applied on the carrier transition, with a π phase shift relative to (a), leading to the operator $V^{1/2}(-\pi/2)$ of Ref. [1].

is as follows:

Input state	→	Output state
$ 0\rangle \downarrow\rangle$	→	$ 0\rangle \downarrow\rangle$
$ 0\rangle \uparrow\rangle$	→	$ 0\rangle \uparrow\rangle$
$ 1\rangle \downarrow\rangle$	→	$ 1\rangle \uparrow\rangle$
$ 1\rangle \uparrow\rangle$	→	$ 1\rangle \downarrow\rangle$

(2)

The experiment apparatus is described elsewhere [16,17]. A single ${}^9\text{Be}^+$ ion is stored in a coaxial-resonator rf-ion trap [17], which provides pseudopotential oscillation frequencies of $(\omega_x, \omega_y, \omega_z)/2\pi \approx (11.2, 18.2, 29.8)$ MHz along the principal axes of the trap. We cool the ion so that the $n_x = 0$ vibrational ground state is occupied $\approx 95\%$ of the time by employing resolved-sideband stimulated Raman cooling in the x dimension, exactly as in Ref. [16]. The two Raman beams each contain ≈ 1 mW of power at ≈ 313 nm and are detuned ≈ 50 GHz red of the ${}^2P_{1/2}$ excited state. The Raman beams are applied to the ion in directions such that their wave-vector difference $\delta\mathbf{k}$ points nearly along the x axis of the trap; thus the Raman transitions are highly insensitive to motion in the other two dimensions. The Lamb-Dicke parameter is $\eta_x = \delta k x_0 \approx 0.2$, where $x_0 \approx 7$ nm is the spread of the $n_x = 0$ wave function. The carrier ($|n\rangle|\downarrow\rangle \rightarrow |n\rangle|\uparrow\rangle$) Rabi frequency is $\Omega_0 2\pi \approx 140$ kHz, the red ($|1\rangle|\downarrow\rangle \rightarrow |0\rangle|\uparrow\rangle$) and blue ($|0\rangle|\downarrow\rangle \rightarrow |1\rangle|\uparrow\rangle$) sideband Rabi frequencies are $\eta_x \Omega_0 / 2\pi \approx 30$ kHz, and the auxiliary transition ($|1\rangle|\uparrow\rangle \rightarrow |0\rangle|\downarrow\rangle$) Rabi frequency is $\eta_x \Omega_{\text{aux}} / 2\pi \approx 12$ kHz. The difference frequency of the Raman beams is tunable from 1200 to 1300 MHz with the use of a double pass acousto-optic modulator (AOM), and the Raman pulse durations are controlled with additional switching AOMs. Since the Raman beams are generated from a single laser and an AOM, broadening of the Raman transitions due to a finite laser linewidth is negligible [18].

Following Raman cooling to the $|0\rangle|\downarrow\rangle$ state, but before application of the CN operation, we apply appropriately

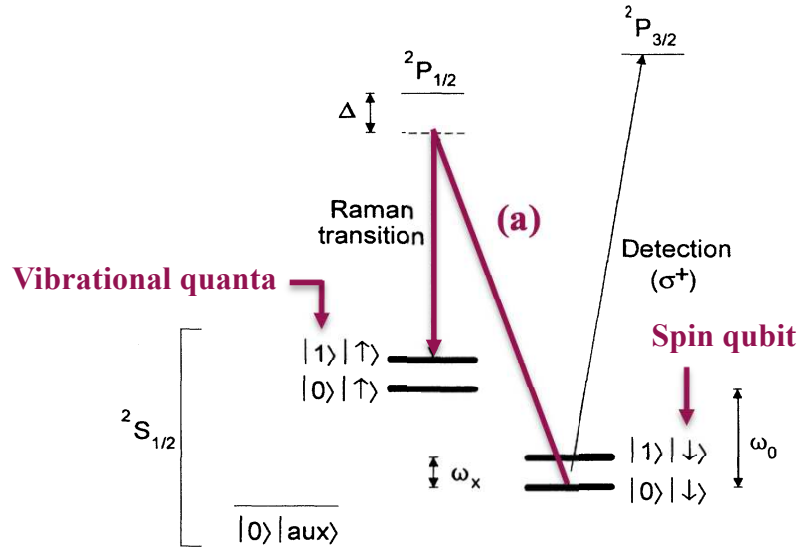


FIG. 1. ${}^9\text{Be}^+$ energy levels. The levels indicated with thick lines form the basis of the quantum register: internal levels are $|S\rangle = |\downarrow\rangle$ and $|\uparrow\rangle$ (${}^2S_{1/2}|F=2, m_F=2\rangle$ and ${}^2S_{1/2}|F=1, m_F=1\rangle$ levels, respectively, separated by $\omega_0/2\pi \approx 1.250$ GHz), and $|\text{aux}\rangle = {}^2S_{1/2}|F=2, m_F=0\rangle$ (separated from $|\downarrow\rangle$ by ≈ 2.5 MHz); external vibrational levels are $|n\rangle = |0\rangle$ and $|1\rangle$ (separated by $\omega_x/2\pi \approx 11.2$ MHz). Stimulated Raman transitions between ${}^2S_{1/2}$ hyperfine states are driven through the virtual ${}^2P_{1/2}$ level ($\Delta \approx 50$ GHz) with a pair of ≈ 313 nm laser beams. Measurement of S is accomplished by driving the cycling $|\downarrow\rangle \rightarrow {}^2P_{3/2}|F=3, m_F=3\rangle$ transition with σ^+ -polarized light and detecting the resulting ion fluorescence.

according to the following format:

- A $\pi/2$ pulse is applied on the carrier transition. The effect is described by the operator $V^{1/2}(\pi/2)$ in the notation of Ref. [1].
- A 2π pulse is applied on the blue sideband transition between $|\uparrow\rangle$ and an auxiliary atomic level $|\text{aux}\rangle$ (see Fig. 1).
- A $\pi/2$ pulse is applied on the carrier transition, with a π phase shift relative to (a), leading to the operator $V^{1/2}(-\pi/2)$ of Ref. [1].

is as follows:

Input state	Output state	
$ 0\rangle \downarrow\rangle$	$\rightarrow 0\rangle \downarrow\rangle$	
$ 0\rangle \uparrow\rangle$	$\rightarrow 0\rangle \uparrow\rangle$	(2)
$ 1\rangle \downarrow\rangle$	$\rightarrow 1\rangle \uparrow\rangle$	
$ 1\rangle \uparrow\rangle$	$\rightarrow 1\rangle \downarrow\rangle$	

The experiment apparatus is described elsewhere [16,17]. A single ${}^9\text{Be}^+$ ion is stored in a coaxial-resonator rf-ion trap [17], which provides pseudopotential oscillation frequencies of $(\omega_x, \omega_y, \omega_z)/2\pi \approx (11.2, 18.2, 29.8)$ MHz along the principal axes of the trap. We cool the ion so that the $n_x = 0$ vibrational ground state is occupied $\approx 95\%$ of the time by employing resolved-sideband stimulated Raman cooling in the x dimension, exactly as in Ref. [16]. The two Raman beams each contain ≈ 1 mW of power at ≈ 313 nm and are detuned ≈ 50 GHz red of the ${}^2P_{1/2}$ excited state. The Raman beams are applied to the ion in directions such that their wave-vector difference $\delta\mathbf{k}$ points nearly along the x axis of the trap; thus the Raman transitions are highly insensitive to motion in the other two dimensions. The Lamb-Dicke parameter is $\eta_x = \delta k x_0 \approx 0.2$, where $x_0 \approx 7$ nm is the spread of the $n_x = 0$ wave function. The carrier ($|n\rangle|\downarrow\rangle \rightarrow |n\rangle|\uparrow\rangle$) Rabi frequency is $\Omega_0 2\pi \approx 140$ kHz, the red ($|1\rangle|\downarrow\rangle \rightarrow |0\rangle|\uparrow\rangle$) and blue ($|0\rangle|\downarrow\rangle \rightarrow |1\rangle|\uparrow\rangle$) sideband Rabi frequencies are $\eta_x \Omega_0 / 2\pi \approx 30$ kHz, and the auxiliary transition ($|1\rangle|\uparrow\rangle \rightarrow |0\rangle|\downarrow\rangle$) Rabi frequency is $\eta_x \Omega_{\text{aux}} / 2\pi \approx 12$ kHz. The difference frequency of the Raman beams is tunable from 1200 to 1300 MHz with the use of a double pass acousto-optic modulator (AOM), and the Raman pulse durations are controlled with additional switching AOMs. Since the Raman beams are generated from a single laser and an AOM, broadening of the Raman transitions due to a finite laser linewidth is negligible [18].

Following Raman cooling to the $|0\rangle|\downarrow\rangle$ state, but before application of the CN operation, we apply appropriately

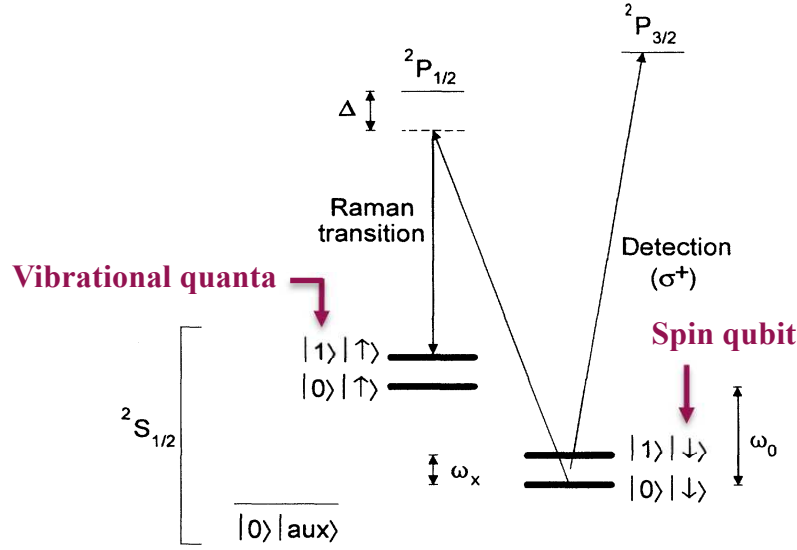


FIG. 1. ${}^9\text{Be}^+$ energy levels. The levels indicated with thick lines form the basis of the quantum register: internal levels are $|S\rangle = |\downarrow\rangle$ and $|\uparrow\rangle$ (${}^2S_{1/2}|F=2, m_F=2\rangle$ and ${}^2S_{1/2}|F=1, m_F=1\rangle$ levels, respectively, separated by $\omega_0/2\pi \approx 1.250$ GHz), and $|\text{aux}\rangle = {}^2S_{1/2}|F=2, m_F=0\rangle$ (separated from $|\downarrow\rangle$ by ≈ 2.5 MHz); external vibrational levels are $|n\rangle = |0\rangle$ and $|1\rangle$ (separated by $\omega_x/2\pi \approx 11.2$ MHz). Stimulated Raman transitions between ${}^2S_{1/2}$ hyperfine states are driven through the virtual ${}^2P_{1/2}$ level ($\Delta \approx 50$ GHz) with a pair of ≈ 313 nm laser beams. Measurement of S is accomplished by driving the cycling $|\downarrow\rangle \rightarrow {}^2P_{3/2}|F=3, m_F=3\rangle$ transition with σ^+ -polarized light and detecting the resulting ion fluorescence.

according to the following format:

- A $\pi/2$ pulse is applied on the carrier transition. The effect is described by the operator $V^{1/2}(\pi/2)$ in the notation of Ref. [1].
- A 2π pulse is applied on the blue sideband transition between $|\uparrow\rangle$ and an auxiliary atomic level $|\text{aux}\rangle$ (see Fig. 1).
- A $\pi/2$ pulse is applied on the carrier transition, with a π phase shift relative to (a), leading to the operator $V^{1/2}(-\pi/2)$ of Ref. [1].

is as follows:

Input state	→	Output state
$ 0\rangle \downarrow\rangle$	→	$ 0\rangle \downarrow\rangle$
$ 0\rangle \uparrow\rangle$	→	$ 0\rangle \uparrow\rangle$
$ 1\rangle \downarrow\rangle$	→	$ 1\rangle \uparrow\rangle$
$ 1\rangle \uparrow\rangle$	→	$ 1\rangle \downarrow\rangle$

(2)

The experiment apparatus is described elsewhere [16,17]. A single ${}^9\text{Be}^+$ ion is stored in a coaxial-resonator rf-ion trap [17], which provides pseudopotential oscillation frequencies of $(\omega_x, \omega_y, \omega_z)/2\pi \approx (11.2, 18.2, 29.8)$ MHz along the principal axes of the trap. We cool the ion so that the $n_x = 0$ vibrational ground state is occupied $\approx 95\%$ of the time by employing resolved-sideband stimulated Raman cooling in the x dimension, exactly as in Ref. [16]. The two Raman beams each contain ≈ 1 mW of power at ≈ 313 nm and are detuned ≈ 50 GHz red of the ${}^2P_{1/2}$ excited state. The Raman beams are applied to the ion in directions such that their wave-vector difference $\delta\mathbf{k}$ points nearly along the x axis of the trap; thus the Raman transitions are highly insensitive to motion in the other two dimensions. The Lamb-Dicke parameter is $\eta_x = \delta k x_0 \approx 0.2$, where $x_0 \approx 7$ nm is the spread of the $n_x = 0$ wave function. The carrier ($|n\rangle|\downarrow\rangle \rightarrow |n\rangle|\uparrow\rangle$) Rabi frequency is $\Omega_0 2\pi \approx 140$ kHz, the red ($|1\rangle|\downarrow\rangle \rightarrow |0\rangle|\uparrow\rangle$) and blue ($|0\rangle|\downarrow\rangle \rightarrow |1\rangle|\uparrow\rangle$) sideband Rabi frequencies are $\eta_x \Omega_0 / 2\pi \approx 30$ kHz, and the auxiliary transition ($|1\rangle|\uparrow\rangle \rightarrow |0\rangle|\downarrow\rangle$) Rabi frequency is $\eta_x \Omega_{\text{aux}} / 2\pi \approx 12$ kHz. The difference frequency of the Raman beams is tunable from 1200 to 1300 MHz with the use of a double pass acousto-optic modulator (AOM), and the Raman pulse durations are controlled with additional switching AOMs. Since the Raman beams are generated from a single laser and an AOM, broadening of the Raman transitions due to a finite laser linewidth is negligible [18].

Following Raman cooling to the $|0\rangle|\downarrow\rangle$ state, but before application of the CN operation, we apply appropriately

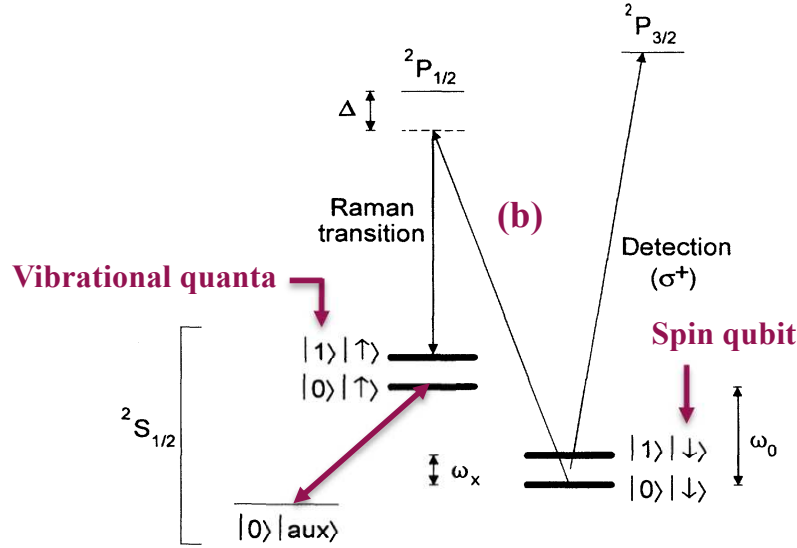


FIG. 1. ${}^9\text{Be}^+$ energy levels. The levels indicated with thick lines form the basis of the quantum register: internal levels are $|S\rangle = |\downarrow\rangle$ and $|\uparrow\rangle$ (${}^2S_{1/2}|F=2, m_F=2\rangle$ and ${}^2S_{1/2}|F=1, m_F=1\rangle$ levels, respectively, separated by $\omega_0/2\pi \approx 1.250$ GHz), and $|\text{aux}\rangle = {}^2S_{1/2}|F=2, m_F=0\rangle$ (separated from $|\downarrow\rangle$ by ≈ 2.5 MHz); external vibrational levels are $|n\rangle = |0\rangle$ and $|1\rangle$ (separated by $\omega_x/2\pi \approx 11.2$ MHz). Stimulated Raman transitions between ${}^2S_{1/2}$ hyperfine states are driven through the virtual ${}^2P_{1/2}$ level ($\Delta \approx 50$ GHz) with a pair of ≈ 313 nm laser beams. Measurement of S is accomplished by driving the cycling $|\downarrow\rangle \rightarrow {}^2P_{3/2}|F=3, m_F=3\rangle$ transition with σ^+ -polarized light and detecting the resulting ion fluorescence.

according to the following format:

- A $\pi/2$ pulse is applied on the carrier transition. The effect is described by the operator $V^{1/2}(\pi/2)$ in the notation of Ref. [1].
- A 2π pulse is applied on the blue sideband transition between $|\uparrow\rangle$ and an auxiliary atomic level $|\text{aux}\rangle$ (see Fig. 1).
- A $\pi/2$ pulse is applied on the carrier transition, with a π phase shift relative to (a), leading to the operator $V^{1/2}(-\pi/2)$ of Ref. [1].

is as follows:

Input state	→	Output state
$ 0\rangle \downarrow\rangle$	→	$ 0\rangle \downarrow\rangle$
$ 0\rangle \uparrow\rangle$	→	$ 0\rangle \uparrow\rangle$
$ 1\rangle \downarrow\rangle$	→	$ 1\rangle \uparrow\rangle$
$ 1\rangle \uparrow\rangle$	→	$ 1\rangle \downarrow\rangle$

(2)

The experiment apparatus is described elsewhere [16,17]. A single ${}^9\text{Be}^+$ ion is stored in a coaxial-resonator rf-ion trap [17], which provides pseudopotential oscillation frequencies of $(\omega_x, \omega_y, \omega_z)/2\pi \approx (11.2, 18.2, 29.8)$ MHz along the principal axes of the trap. We cool the ion so that the $n_x = 0$ vibrational ground state is occupied $\approx 95\%$ of the time by employing resolved-sideband stimulated Raman cooling in the x dimension, exactly as in Ref. [16]. The two Raman beams each contain ≈ 1 mW of power at ≈ 313 nm and are detuned ≈ 50 GHz red of the ${}^2P_{1/2}$ excited state. The Raman beams are applied to the ion in directions such that their wave-vector difference $\delta\mathbf{k}$ points nearly along the x axis of the trap; thus the Raman transitions are highly insensitive to motion in the other two dimensions. The Lamb-Dicke parameter is $\eta_x = \delta k x_0 \approx 0.2$, where $x_0 \approx 7$ nm is the spread of the $n_x = 0$ wave function. The carrier ($|n\rangle|\downarrow\rangle \rightarrow |n\rangle|\uparrow\rangle$) Rabi frequency is $\Omega_0 2\pi \approx 140$ kHz, the red ($|1\rangle|\downarrow\rangle \rightarrow |0\rangle|\uparrow\rangle$) and blue ($|0\rangle|\downarrow\rangle \rightarrow |1\rangle|\uparrow\rangle$) sideband Rabi frequencies are $\eta_x \Omega_0 / 2\pi \approx 30$ kHz, and the auxiliary transition ($|1\rangle|\uparrow\rangle \rightarrow |0\rangle|\downarrow\rangle$) Rabi frequency is $\eta_x \Omega_{\text{aux}} / 2\pi \approx 12$ kHz. The difference frequency of the Raman beams is tunable from 1200 to 1300 MHz with the use of a double pass acousto-optic modulator (AOM), and the Raman pulse durations are controlled with additional switching AOMs. Since the Raman beams are generated from a single laser and an AOM, broadening of the Raman transitions due to a finite laser linewidth is negligible [18].

Following Raman cooling to the $|0\rangle|\downarrow\rangle$ state, but before application of the CN operation, we apply appropriately

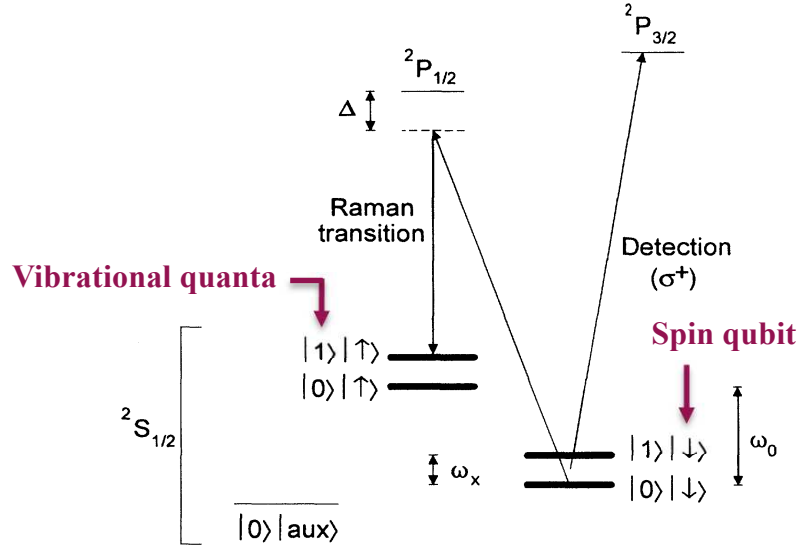


FIG. 1. ${}^9\text{Be}^+$ energy levels. The levels indicated with thick lines form the basis of the quantum register: internal levels are $|S\rangle = |\downarrow\rangle$ and $|\uparrow\rangle$ (${}^2S_{1/2}|F=2, m_F=2\rangle$ and ${}^2S_{1/2}|F=1, m_F=1\rangle$ levels, respectively, separated by $\omega_0/2\pi \approx 1.250$ GHz), and $|\text{aux}\rangle = {}^2S_{1/2}|F=2, m_F=0\rangle$ (separated from $|\downarrow\rangle$ by ≈ 2.5 MHz); external vibrational levels are $|n\rangle = |0\rangle$ and $|1\rangle$ (separated by $\omega_x/2\pi \approx 11.2$ MHz). Stimulated Raman transitions between ${}^2S_{1/2}$ hyperfine states are driven through the virtual ${}^2P_{1/2}$ level ($\Delta \approx 50$ GHz) with a pair of ≈ 313 nm laser beams. Measurement of S is accomplished by driving the cycling $|\downarrow\rangle \rightarrow {}^2P_{3/2}|F=3, m_F=3\rangle$ transition with σ^+ -polarized light and detecting the resulting ion fluorescence.

according to the following format:

- A $\pi/2$ pulse is applied on the carrier transition. The effect is described by the operator $V^{1/2}(\pi/2)$ in the notation of Ref. [1].
- A 2π pulse is applied on the blue sideband transition between $|\uparrow\rangle$ and an auxiliary atomic level $|\text{aux}\rangle$ (see Fig. 1).
- A $\pi/2$ pulse is applied on the carrier transition, with a π phase shift relative to (a), leading to the operator $V^{1/2}(-\pi/2)$ of Ref. [1].

is as follows:

Input state	Output state	
$ 0\rangle \downarrow\rangle$	$\rightarrow 0\rangle \downarrow\rangle$	
$ 0\rangle \uparrow\rangle$	$\rightarrow 0\rangle \uparrow\rangle$	(2)
$ 1\rangle \downarrow\rangle$	$\rightarrow 1\rangle \uparrow\rangle$	
$ 1\rangle \uparrow\rangle$	$\rightarrow 1\rangle \downarrow\rangle$	

The experiment apparatus is described elsewhere [16,17]. A single ${}^9\text{Be}^+$ ion is stored in a coaxial-resonator rf-ion trap [17], which provides pseudopotential oscillation frequencies of $(\omega_x, \omega_y, \omega_z)/2\pi \approx (11.2, 18.2, 29.8)$ MHz along the principal axes of the trap. We cool the ion so that the $n_x = 0$ vibrational ground state is occupied $\approx 95\%$ of the time by employing resolved-sideband stimulated Raman cooling in the x dimension, exactly as in Ref. [16]. The two Raman beams each contain ≈ 1 mW of power at ≈ 313 nm and are detuned ≈ 50 GHz red of the ${}^2P_{1/2}$ excited state. The Raman beams are applied to the ion in directions such that their wave-vector difference $\delta\mathbf{k}$ points nearly along the x axis of the trap; thus the Raman transitions are highly insensitive to motion in the other two dimensions. The Lamb-Dicke parameter is $\eta_x = \delta k x_0 \approx 0.2$, where $x_0 \approx 7$ nm is the spread of the $n_x = 0$ wave function. The carrier ($|n\rangle|\downarrow\rangle \rightarrow |n\rangle|\uparrow\rangle$) Rabi frequency is $\Omega_0 2\pi \approx 140$ kHz, the red ($|1\rangle|\downarrow\rangle \rightarrow |0\rangle|\uparrow\rangle$) and blue ($|0\rangle|\downarrow\rangle \rightarrow |1\rangle|\uparrow\rangle$) sideband Rabi frequencies are $\eta_x \Omega_0 / 2\pi \approx 30$ kHz, and the auxiliary transition ($|1\rangle|\uparrow\rangle \rightarrow |0\rangle|\downarrow\rangle$) Rabi frequency is $\eta_x \Omega_{\text{aux}} / 2\pi \approx 12$ kHz. The difference frequency of the Raman beams is tunable from 1200 to 1300 MHz with the use of a double pass acousto-optic modulator (AOM), and the Raman pulse durations are controlled with additional switching AOMs. Since the Raman beams are generated from a single laser and an AOM, broadening of the Raman transitions due to a finite laser linewidth is negligible [18].

Following Raman cooling to the $|0\rangle|\downarrow\rangle$ state, but before application of the CN operation, we apply appropriately

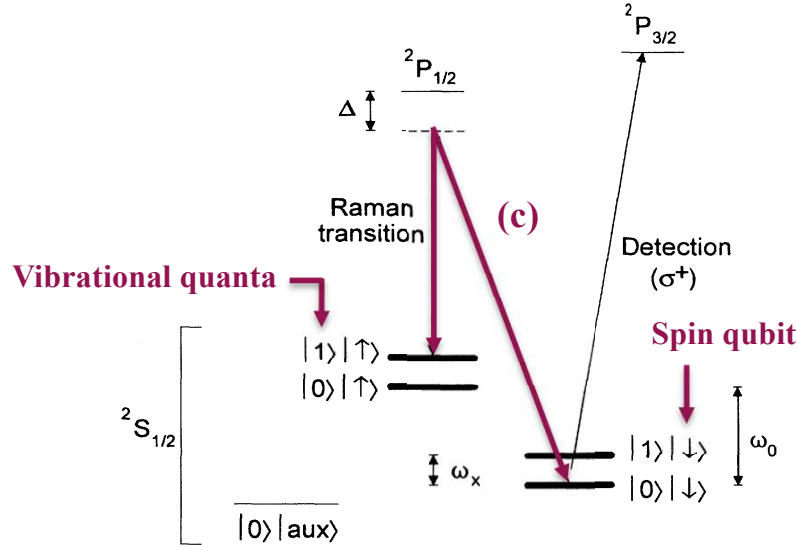


FIG. 1. ${}^9\text{Be}^+$ energy levels. The levels indicated with thick lines form the basis of the quantum register: internal levels are $|S\rangle = |\downarrow\rangle$ and $|\uparrow\rangle$ (${}^2S_{1/2}|F=2, m_F=2\rangle$ and ${}^2S_{1/2}|F=1, m_F=1\rangle$ levels, respectively, separated by $\omega_0/2\pi \approx 1.250$ GHz), and $|\text{aux}\rangle = {}^2S_{1/2}|F=2, m_F=0\rangle$ (separated from $|\downarrow\rangle$ by ≈ 2.5 MHz); external vibrational levels are $|n\rangle = |0\rangle$ and $|1\rangle$ (separated by $\omega_x/2\pi \approx 11.2$ MHz). Stimulated Raman transitions between ${}^2S_{1/2}$ hyperfine states are driven through the virtual ${}^2P_{1/2}$ level ($\Delta \approx 50$ GHz) with a pair of ≈ 313 nm laser beams. Measurement of S is accomplished by driving the cycling $|\downarrow\rangle \rightarrow {}^2P_{3/2}|F=3, m_F=3\rangle$ transition with σ^+ -polarized light and detecting the resulting ion fluorescence.

according to the following format:

- A $\pi/2$ pulse is applied on the carrier transition. The effect is described by the operator $V^{1/2}(\pi/2)$ in the notation of Ref. [1].
- A 2π pulse is applied on the blue sideband transition between $|\uparrow\rangle$ and an auxiliary atomic level $|\text{aux}\rangle$ (see Fig. 1).
- A $\pi/2$ pulse is applied on the carrier transition, with a π phase shift relative to (a), leading to the operator $V^{1/2}(-\pi/2)$ of Ref. [1].

is as follows:

Input state	→	Output state
$ 0\rangle \downarrow\rangle$	→	$ 0\rangle \downarrow\rangle$
$ 0\rangle \uparrow\rangle$	→	$ 0\rangle \uparrow\rangle$
$ 1\rangle \downarrow\rangle$	→	$ 1\rangle \uparrow\rangle$
$ 1\rangle \uparrow\rangle$	→	$ 1\rangle \downarrow\rangle$

(2)

The experiment apparatus is described elsewhere [16,17]. A single ${}^9\text{Be}^+$ ion is stored in a coaxial-resonator rf-ion trap [17], which provides pseudopotential oscillation frequencies of $(\omega_x, \omega_y, \omega_z)/2\pi \approx (11.2, 18.2, 29.8)$ MHz along the principal axes of the trap. We cool the ion so that the $n_x = 0$ vibrational ground state is occupied $\approx 95\%$ of the time by employing resolved-sideband stimulated Raman cooling in the x dimension, exactly as in Ref. [16]. The two Raman beams each contain ≈ 1 mW of power at ≈ 313 nm and are detuned ≈ 50 GHz red of the ${}^2P_{1/2}$ excited state. The Raman beams are applied to the ion in directions such that their wave-vector difference $\delta\mathbf{k}$ points nearly along the x axis of the trap; thus the Raman transitions are highly insensitive to motion in the other two dimensions. The Lamb-Dicke parameter is $\eta_x = \delta k x_0 \approx 0.2$, where $x_0 \approx 7$ nm is the spread of the $n_x = 0$ wave function. The carrier ($|n\rangle|\downarrow\rangle \rightarrow |n\rangle|\uparrow\rangle$) Rabi frequency is $\Omega_0 2\pi \approx 140$ kHz, the red ($|1\rangle|\downarrow\rangle \rightarrow |0\rangle|\uparrow\rangle$) and blue ($|0\rangle|\downarrow\rangle \rightarrow |1\rangle|\uparrow\rangle$) sideband Rabi frequencies are $\eta_x \Omega_0 / 2\pi \approx 30$ kHz, and the auxiliary transition ($|1\rangle|\uparrow\rangle \rightarrow |0\rangle|\downarrow\rangle$) Rabi frequency is $\eta_x \Omega_{\text{aux}} / 2\pi \approx 12$ kHz. The difference frequency of the Raman beams is tunable from 1200 to 1300 MHz with the use of a double pass acousto-optic modulator (AOM), and the Raman pulse durations are controlled with additional switching AOMs. Since the Raman beams are generated from a single laser and an AOM, broadening of the Raman transitions due to a finite laser linewidth is negligible [18].

Following Raman cooling to the $|0\rangle|\downarrow\rangle$ state, but before application of the CN operation, we apply appropriately

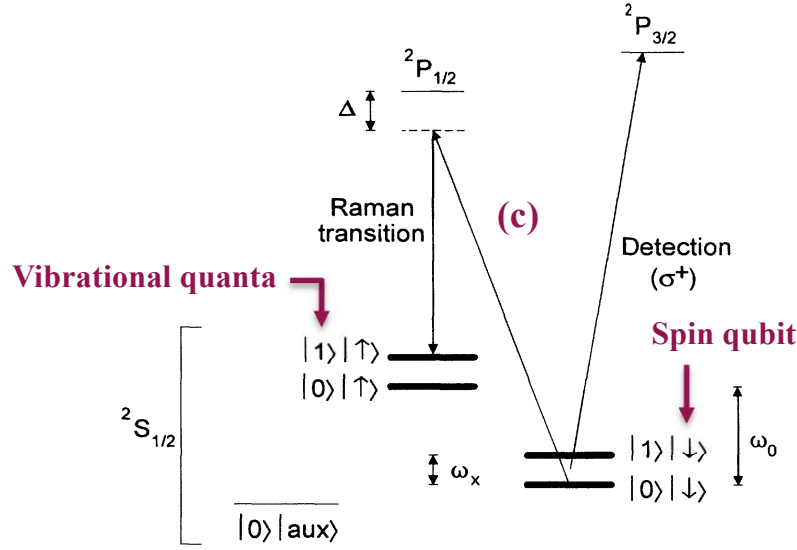


FIG. 1. ${}^9\text{Be}^+$ energy levels. The levels indicated with thick lines form the basis of the quantum register: internal levels are $|S\rangle = |\downarrow\rangle$ and $|\uparrow\rangle$ (${}^2S_{1/2}|F=2, m_F=2\rangle$ and ${}^2S_{1/2}|F=1, m_F=1\rangle$ levels, respectively, separated by $\omega_0/2\pi \approx 1.250$ GHz), and $|\text{aux}\rangle = {}^2S_{1/2}|F=2, m_F=0\rangle$ (separated from $|\downarrow\rangle$ by ≈ 2.5 MHz); external vibrational levels are $|n\rangle = |0\rangle$ and $|1\rangle$ (separated by $\omega_x/2\pi \approx 11.2$ MHz). Stimulated Raman transitions between ${}^2S_{1/2}$ hyperfine states are driven through the virtual ${}^2P_{1/2}$ level ($\Delta \approx 50$ GHz) with a pair of ≈ 313 nm laser beams. Measurement of S is accomplished by driving the cycling $|\downarrow\rangle \rightarrow {}^2P_{3/2}|F=3, m_F=3\rangle$ transition with σ^+ -polarized light and detecting the resulting ion fluorescence.

according to the following format:

- A $\pi/2$ pulse is applied on the carrier transition. The effect is described by the operator $V^{1/2}(\pi/2)$ in the notation of Ref. [1].
- A 2π pulse is applied on the blue sideband transition between $|\uparrow\rangle$ and an auxiliary atomic level $|\text{aux}\rangle$ (see Fig. 1).
- A $\pi/2$ pulse is applied on the carrier transition, with a π phase shift relative to (a), leading to the operator $V^{1/2}(-\pi/2)$ of Ref. [1].

is as follows:

Input state	→	Output state
$ 0\rangle \downarrow\rangle$	→	$ 0\rangle \downarrow\rangle$
$ 0\rangle \uparrow\rangle$	→	$ 0\rangle \uparrow\rangle$
$ 1\rangle \downarrow\rangle$	→	$ 1\rangle \uparrow\rangle$
$ 1\rangle \uparrow\rangle$	→	$ 1\rangle \downarrow\rangle$

(2)

The experiment apparatus is described elsewhere [16,17]. A single ${}^9\text{Be}^+$ ion is stored in a coaxial-resonator rf-ion trap [17], which provides pseudopotential oscillation frequencies of $(\omega_x, \omega_y, \omega_z)/2\pi \approx (11.2, 18.2, 29.8)$ MHz along the principal axes of the trap. We cool the ion so that the $n_x = 0$ vibrational ground state is occupied $\approx 95\%$ of the time by employing resolved-sideband stimulated Raman cooling in the x dimension, exactly as in Ref. [16]. The two Raman beams each contain ≈ 1 mW of power at ≈ 313 nm and are detuned ≈ 50 GHz red of the ${}^2P_{1/2}$ excited state. The Raman beams are applied to the ion in directions such that their wave-vector difference $\delta\mathbf{k}$ points nearly along the x axis of the trap; thus the Raman transitions are highly insensitive to motion in the other two dimensions. The Lamb-Dicke parameter is $\eta_x = \delta k x_0 \approx 0.2$, where $x_0 \approx 7$ nm is the spread of the $n_x = 0$ wave function. The carrier ($|n\rangle|\downarrow\rangle \rightarrow |n\rangle|\uparrow\rangle$) Rabi frequency is $\Omega_0 2\pi \approx 140$ kHz, the red ($|1\rangle|\downarrow\rangle \rightarrow |0\rangle|\uparrow\rangle$) and blue ($|0\rangle|\downarrow\rangle \rightarrow |1\rangle|\uparrow\rangle$) sideband Rabi frequencies are $\eta_x \Omega_0 / 2\pi \approx 30$ kHz, and the auxiliary transition ($|1\rangle|\uparrow\rangle \rightarrow |0\rangle|\downarrow\rangle$) Rabi frequency is $\eta_x \Omega_{\text{aux}} / 2\pi \approx 12$ kHz. The difference frequency of the Raman beams is tunable from 1200 to 1300 MHz with the use of a double pass acousto-optic modulator (AOM), and the Raman pulse durations are controlled with additional switching AOMs. Since the Raman beams are generated from a single laser and an AOM, broadening of the Raman transitions due to a finite laser linewidth is negligible [18].

Following Raman cooling to the $|0\rangle|\downarrow\rangle$ state, but before application of the CN operation, we apply appropriately

Some Benchmarks for Ion Traps

TABLE I. Selected state-of-the-art gate demonstrations.

Gate Type	Gate Method	Fidelity	Gate Time (μs)	Ion Species	Ref.
Single-Qubit	Optical	0.99995	5	$^{40}\text{Ca}^+$	[28]
	Raman	0.99993	7.5	$^{43}\text{Ca}^+$	[27]
	Raman	0.99996	2	$^9\text{Be}^+$	[37]
	Raman	0.99	0.00005	$^{171}\text{Yb}^+$	[163]
	Raman	0.999	8	$^{88}\text{Sr}^+$	[113]
	Microwave	0.999999	12	$^{43}\text{Ca}^+$	[22]
Two-Qubit (1 species)	Microwave		0.0186	$^{25}\text{Mg}^+$	[164]
	Optical	0.996	–	$^{40}\text{Ca}^+$	[38]
	Optical	0.993	50	$^{40}\text{Ca}^+$	[8]
	Raman	0.9991(6)	30	$^9\text{Be}^+$	[37]
	Raman	0.999	100	$^{43}\text{Ca}^+$	[27]
	Raman	0.998	1.6	$^{43}\text{Ca}^+$	[40]
	Raman	0.60	0.5	$^{43}\text{Ca}^+$	[40]
	Microwave	0.997	3250	$^{43}\text{Ca}^+$	[165]
	(AC B-field gradient) Microwave	0.985	2700	$^{171}\text{Yb}^+$	[166]
	(DC B-field gradient)				
Two-Qubit (2 species)	Raman/Raman	0.998(6)	27.4	$^{40}\text{Ca}^+ / ^{43}\text{Ca}^+$	[167]
	Raman/Raman	0.979(1)	35	$^9\text{Be}^+ / ^{25}\text{Mg}^+$	[168]

polarization (or frequency) does not allow it to couple to the ground state, and it cannot be rotated in $|0\rangle_c |n=0\rangle$ because the drive is red-detuned. A final π -pulse on the control ion will return the control ion to its initial state. The resulting state transformation looks like:

$$\begin{aligned}
 |0\rangle_c |0\rangle_t &\rightarrow |0\rangle_c |0\rangle_t & (1) \\
 |0\rangle_c |1\rangle_t &\rightarrow |0\rangle_c |1\rangle_t & (2) \\
 |1\rangle_c |0\rangle_t &\rightarrow |1\rangle_c |0\rangle_t & (3) \\
 |1\rangle_c |1\rangle_t &\rightarrow -|1\rangle_c |1\rangle_t & (4)
 \end{aligned}$$

The gate thus inverts the phase of only the $|1\rangle_c |1\rangle_t$ state, realizing an entangling controlled-phase interaction. Besides cooling to the motional ground state, the CZ gate requires individual addressing of each ion and multiple polarizations for the drive laser. Despite these limitations, a modified CZ interaction was demonstrated the same year it was proposed [4], entangling the internal state and motional state of a single $^9\text{Be}^+$ ion. In 1998, a two-ion entangling gate with fidelity of 0.7 was demonstrated between two Be^+ ions with gate time of $\sim 10 \mu\text{s}$, while a Cirac-Zoller gate and single-qubit rotations were used to implement the CNOT operations on two

The requirement that the ions remain in the motional ground state is a significant limitation on the original Cirac-Zoller proposal. As discussed in Sec. II C 2, even when the ions have been cooled to the motional ground state, they can be subsequently heated by electric-field noise. In 1999, Mølmer and Sørensen introduced a controlled-phase gate which could be implemented without the need to be in the motional ground state [25]. The Mølmer-Sørensen (MS) gate generates a state-dependent force with bichromatic laser fields tuned near first-order sideband transitions. The motional-state wavepacket executes a closed trajectory in phase space, giving rise to a state-dependent geometric phase. At the conclusion of the gate, internal and motional states are disentangled for all values of n . Hence, the MS gate can be used for ions that are not cooled to the motional ground state. An additional feature of the MS interaction is that entanglement among multiple ions can be generated using only global control lasers (that is, it does not require lasers independently focused on each ion). The MS entangling gate was first demonstrated for chains of 2 and 4 Be^+ ions in 2000 [6]. To date, the highest-achieved fidelities in both optical and hyperfine two-qubit gates

Some links to get started

Amazon Braket (IonQ, other Technologies)
<https://aws.amazon.com/braket/>

Quantinuum (Ion Trap Quantum Computing)
<https://www.quantinuum.com>

IonQ <https://ionq.com>

NIST <https://www.nist.gov/pml/time-and-frequency-division/ion-storage>

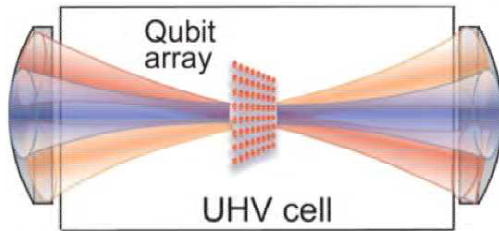
Challenge: Do a web search and look for the largest GHZ state made in the lab

$$|GHZ\rangle = \frac{1}{\sqrt{2}} (|00\dots 00\rangle + |11\dots 11\rangle)$$

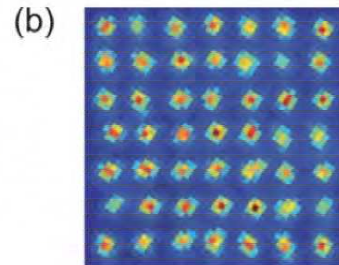
Note: What is the fidelity of the state ?

Neutral Atom based Quantum Processors

Optical tweezer array



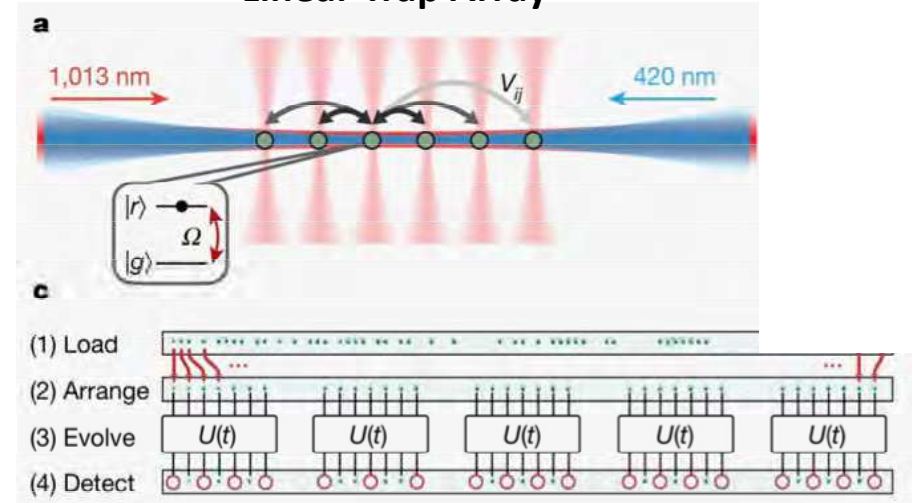
Fluorescing atoms



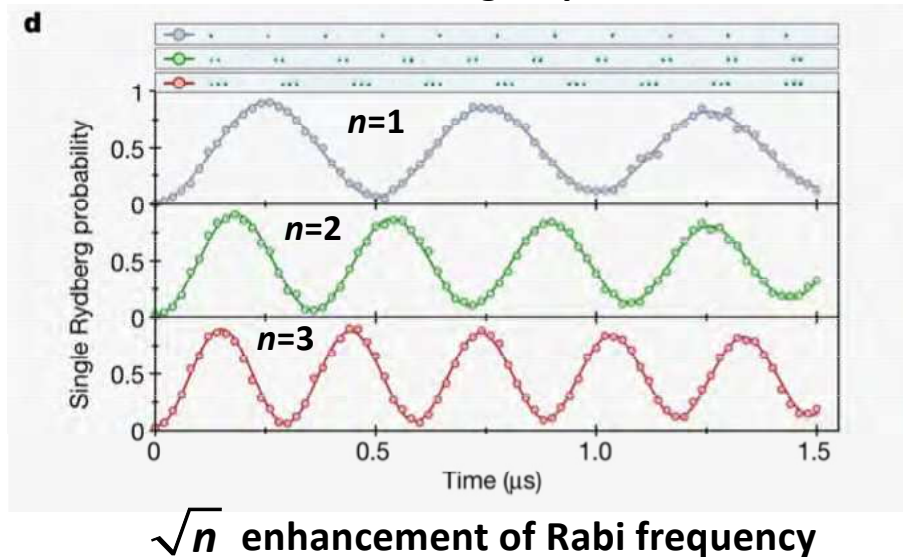
- * Large numbers of non-interacting qubits, (~ 256) trapped in 2D or 3D arrays.
- * Qubits interact when excited into Rydberg states with large dipole moments
- * Major advantage: Weak coupling to the environment when not doing gates
 - ➡ excellent quantum memory
- * Favorite platform for quantum simulation of quantum manybody physics
- * BEC's in optical lattices as analog simulators of superconductivity, quantum magnetism and more

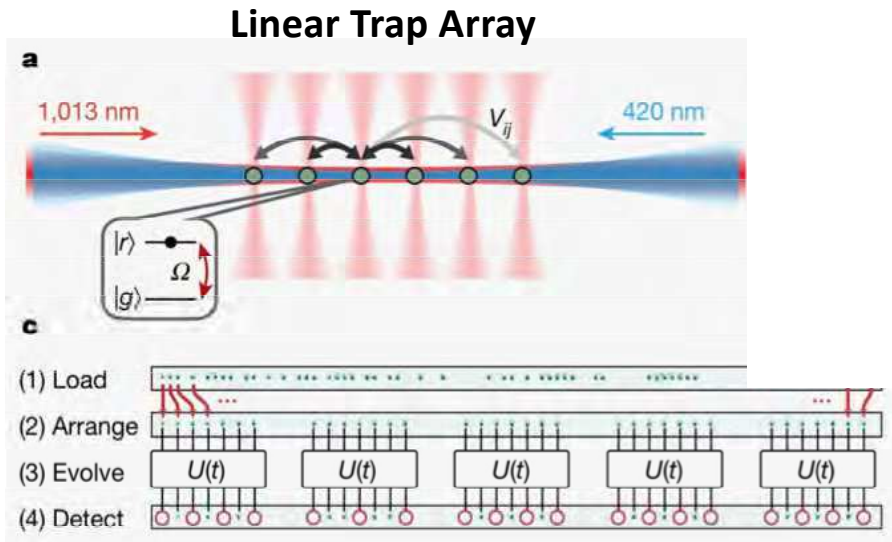
2-photon transition to a Rydberg state

Linear Trap Array

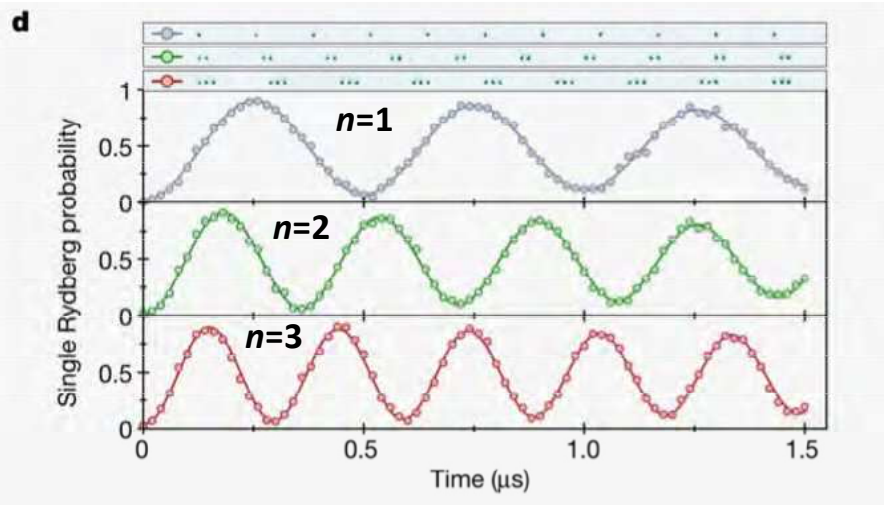


Sorted into groups of n



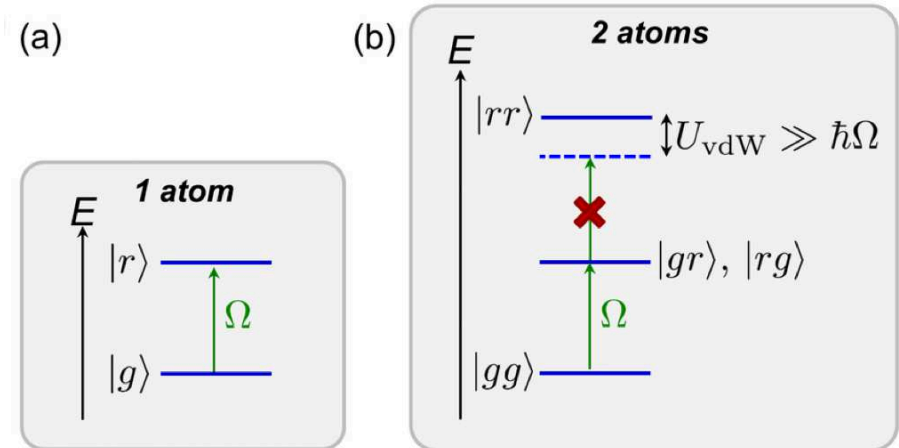


Sorted into groups of n



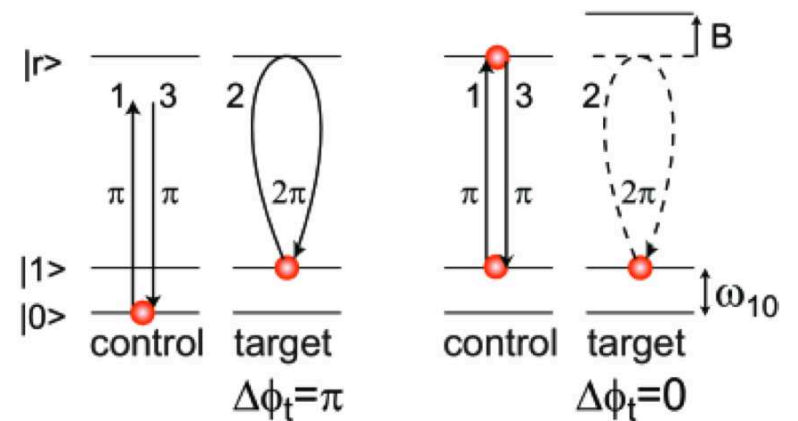
\sqrt{n} enhancement of Rabi frequency

Rydberg Blockade



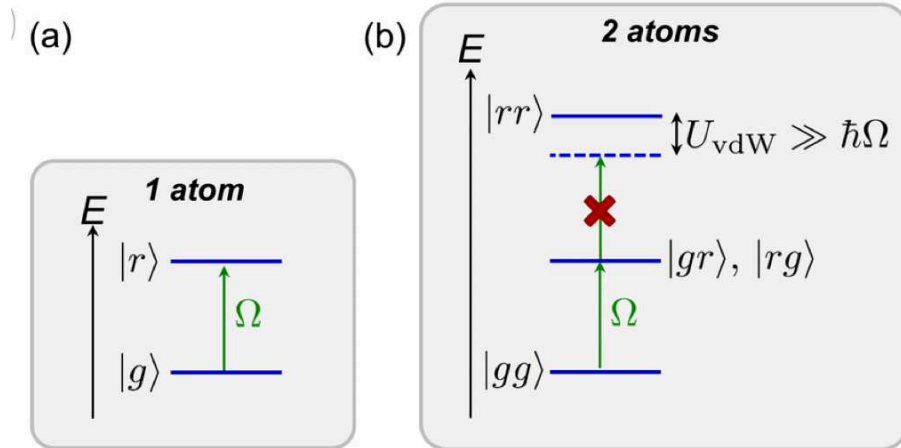
Principle of the Rydberg blockade. (a) A resonant laser couples, with strength Ω , the Rydberg state $|r\rangle$ and the ground state $|g\rangle$ of an atom. (b) For two nearby atoms, interactions U_{vdW} shift the doubly excited state $|rr\rangle$, preventing the double excitation of the atom pair when $U_{\text{vdW}} \gg \hbar\Omega$.

Controlled-Phase Gate



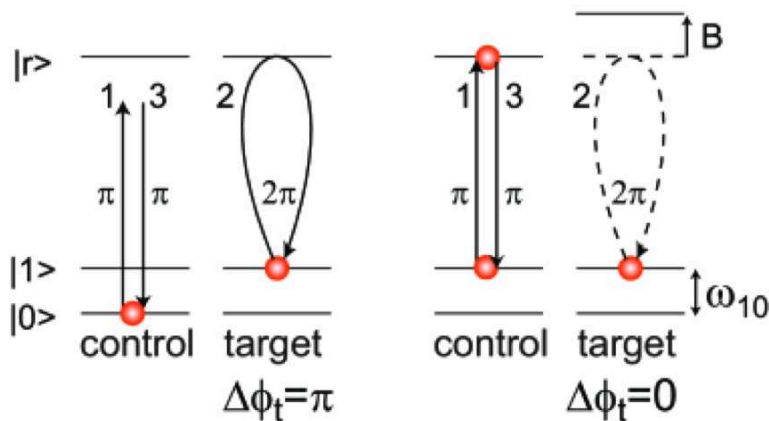
π phase shift of Target conditioned on Control

Rydberg Blockade



Principle of the Rydberg blockade. (a) A resonant laser couples, with strength Ω , the Rydberg state $|r\rangle$ and the ground state $|g\rangle$ of an atom. (b) For two nearby atoms, interactions U_{vdW} shift the doubly excited state $|rr\rangle$, preventing the double excitation of the atom pair when $U_{vdW} \gg \hbar\Omega$.

Controlled-Phase Gate



π phase shift of Target conditioned on Control

Some links to get started

QuEra <https://www.quera.com/aquila>

Cold Quanta <https://coldquanta.com>

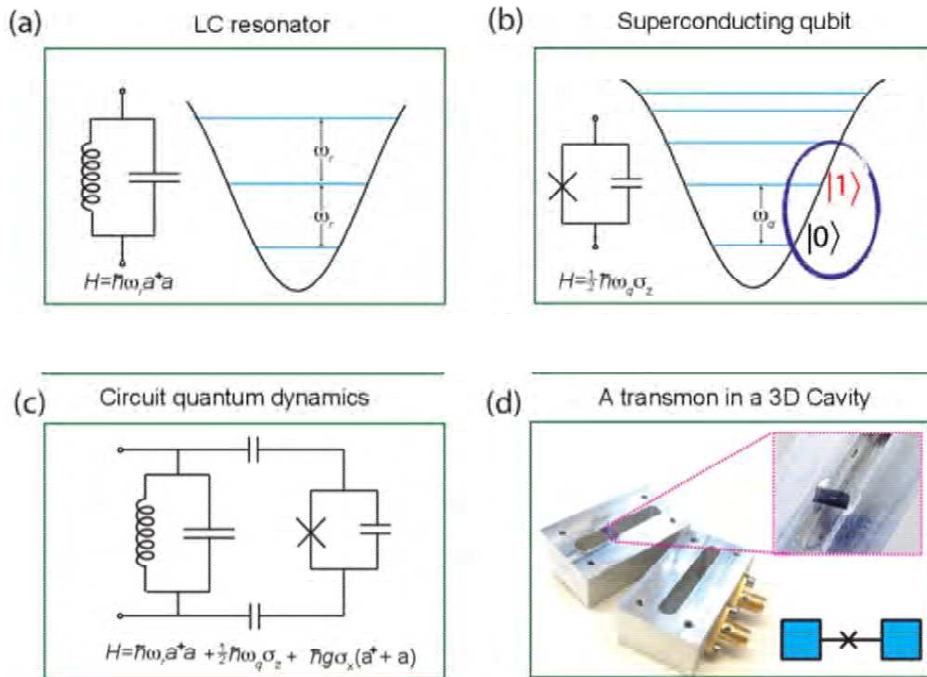
Sandia, Los Alamos National Labs

Individual PI's – Quantum Simulation

Lukin, Vuletic, Greiner, Endres, Bloch, Saffman, Biederman, Browaeys, Weiss, and many, many others...

Superconducting Qubits

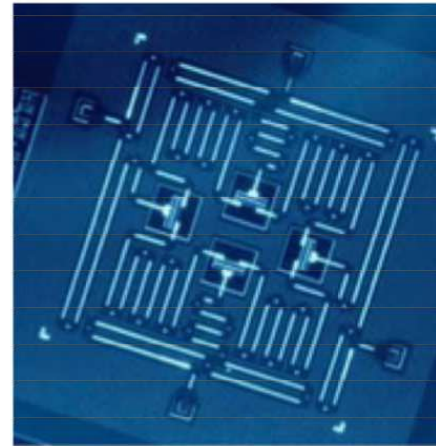
- * The basic building block is the so-called Transmon Qubit
- * A Transmon is a nonlinear oscillator made from a Josephson Junction and other circuit elements



Jaynes-Cummings Hamiltonian

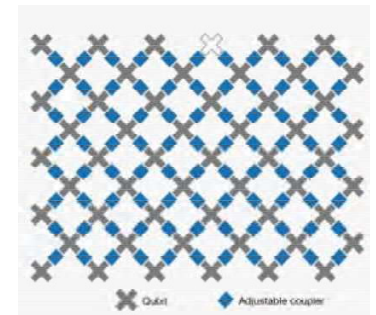
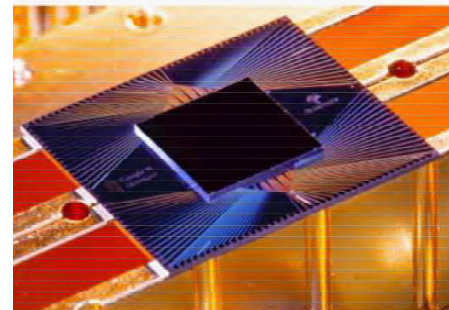
Superconducting Qubits

IBM 4-Transmon device (2017)



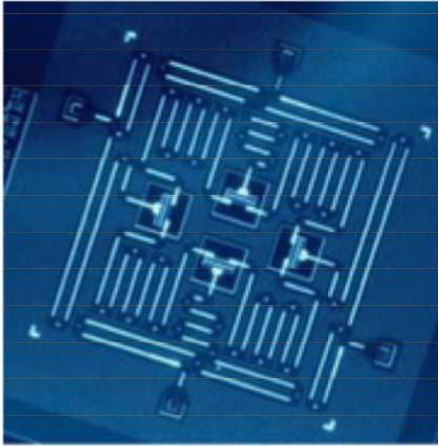
A device consisting of four transmon qubits, four quantum busses, and four readout resonators fabricated by IBM and published in npj Quantum Information in January 2017. [4]

Google 54-Transmon device (2019)



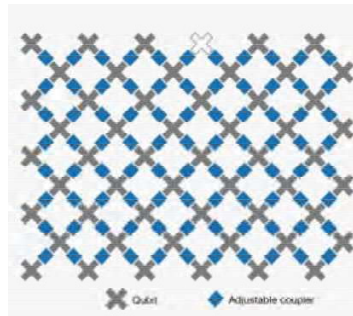
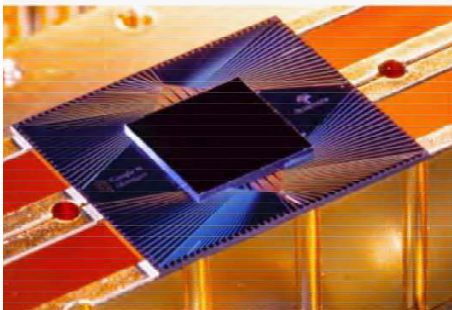
Superconducting Qubits

IBM 4-Transmon device (2017)



A device consisting of four transmon qubits, four quantum busses, and four readout resonators fabricated by IBM and published in npj Quantum Information in January 2017.^[4]

Google 54-Transmon device (2019)



Advantages

- * Solid State platform, looks like electronics
- * Clearer path to scale up to many qubits?

Challenges

- * Gates, coherence times not as good as atomic platforms, but gap is closing
- * Requires dilution refrigerator

Industry Favorite

- * Large efforts at IBM, Google, Rigetti
Cloud Quantum Computing
- * Amazon Braket (IonQ, other Technology)
<https://aws.amazon.com/braket/>